1995

The Presidents' Day cyclone of 1819 February 1979: Influence of upstream trough amplification and associated tropopause folding on rapid cyclogenesis

Uccellini, Louis W.; Keyser, Daniel; Brill, Keith F.; Wash, Carlyle H.

The Presidents' Day Cyclone of 18–19 February 1979: Influence of Upstream Trough Amplification and Associated Tropopause Folding on Rapid Cyclogenesis

LOUIS W. UCCELLINI AND DANIEL KEYSER

Laboratory for Atmospheres, NASA/Goddard Space Flight Center, Greenbelt, MD 20771

KEITH F. BRILL

General Software Corporation, Landover, MD 20785

CARLYLE H. WASH

Department of Meteorology, Naval Postgraduate School, Monterey, CA 93943

ABSTRACT

A diagnostic analysis of an amplifying polar jet–trough system and associated tropopause fold which preceded the 19 February 1979 Presidents' Day cyclone is presented. The analysis is based on conventional radiosonde data, infrared and visible satellite imagery, 6.7 μm water vapor measurements from the Temperature-Humidity Infrared Radiometer (THIR), and ozone measurements from the Total Ozone Mapping Spectrometer (TOMS). The case study indicates that dynamically forced meso-α scale vertical circulations played an important role in the extrusion of stratospheric air along the axis of a polar jet and the subsequent development of the storm system. Specific findings include: 1) Tropopause folding accompanying an amplifying polar jet–trough system occurred along the axis of the intensifying polar jet in response to subsidence forced by geostrophic deformation patterns associated with the jet streak. 2) The folding process extruded dry stratospheric air marked by high values of potential vorticity down toward the 700 mb level, 1500 km upstream of the East Coast, 12 to 24 h prior to the explosive development phase of the cyclone. This result differs from previous case studies which have emphasized the concurrent development of a folded tropopause and cyclogenesis. 3) During the 12 h preceding rapid cyclogenesis, the stratospheric air descended toward the 800 mb level and moved toward the East Coast to a position just upstream of the area in which rapid cyclogenesis occurred. Even though potential vorticity was not strictly conserved, the absolute vorticity increased in the lower to middle troposphere in association with adiabatic mass convergence, vertical stretching, and the related decrease of static stability of the air mass originating in the stratosphere. 4) As was inferred from the infrared and visible satellite imagery and the ozone measurements, the stratospheric air mass was nearly colocated with the storm center as explosive deepening and vortex development occurred, suggesting that the explosive development of the cyclone was likely influenced by the stratospheric air mass as it descended toward a deep oceanic planetary boundary layer immediately off the East Coast.

1. Introduction

On 18–19 February 1979, a major snowstorm developed along the Middle Atlantic Coast, producing heavy snow from North Carolina to southeastern New York and extreme southern New England. Various aspects of this storm, known as the Presidents' Day cyclone, have been described by Bosart (1981), Uccellini et al. (1983, 1984) and Bosart and Lin (1984). Bosart's (1981) study provides a detailed analysis of the coastal frontogenesis that played an important role in concentrating low-level baroclinicity along the coast during the precyclogenetic period on 18 February. Bosart also emphasizes a possible connection between a line of convection near the center of the storm and the onset of explosive cyclogenesis which began after 1200 GMT 19 February. The

Uccellini et al. (1984) study describes the increase in upper-level divergence associated with a significantly ageostrophic subtropical jet streak (STJ) and an intense and highly ageostrophic low-level jet (LLJ), both of which considerably influenced the development of heavy snow during the precyclogenetic period. The synoptic overviews by Bosart (1981) and Uccellini et al. (1984) also indicate that the explosive development phase of the Presidents' Day cyclone commenced as an eastward propagating polar jet (PJ)–trough system moved across the central United States and overtook the coastal front on 19 February. Uccellini et al. (1984) briefly note that a tropopause fold (Reed, 1955; Reed and Danielsen, 1959) developed in the central United States on 18 February 1979, 1500 to 2000 km upstream of the East Coast and 12

to 24 h prior to the explosive cyclogenesis along the East Coast.

The purpose of this paper is to present a more detailed description and complete diagnostic analysis of the PJ–trough system and imbedded tropopause fold and assess its possible role in the overall development of the Presidents' Day cyclone. The diagnostic analysis is similar to others that use the conservation of potential vorticity to establish a link between a folded tropopause and explosive cyclogenesis. However, in this case, the tropopause fold occurred 12 to 24 h prior to cyclogenesis rather than during the cyclogenetic period as has been noted for other cases (e.g., see Staley, 1960; Bleck, 1973, 1974). Thus, the Presidents' Day cyclone provides an opportunity to investigate the sequence of events eventually culminating in the explosive development of the cyclone. This sequence of events involves synoptic-scale dynamical processes that lead to mesoscale transverse ageostrophic circulations and tropopause folding along the axis of the PJ and the subsequent association of the stratospheric extrusion with rapid cyclogenesis.

The analysis of the scale interactions is based not only on radiosonde data but also on important new data sources for studying tropopause folds: the Total Ozone Mapping Spectrometer (TOMS) and the 6.7 μm water vapor channel on the Temperature–Humidity Infrared Radiometer (THIR) flown aboard the Nimbus 7 polar-orbiting satellite. Both the radiosonde and TOMS data have limitations which prevent a complete description of the dynamical processes that link tropopause folding directly to rapid cyclogenesis. The 12-h sampling interval in the radiosonde data reduces the capability of describing the rapidly changing structure of cyclones, which was recognized over 30 years ago by Palmén (1951). The TOMS data are also limited in that the ozone measurements are available only once per day. Nevertheless, combining the radiosonde measurements and the THIR, TOMS and other satellite imagery provides a wealth of data to study the evolution of stratospheric extrusions prior to and during the development of cyclones.

A review of the Presidents' Day cyclone and description of the satellite imagery are presented in Section 2. A description of the well-known synoptic-scale characteristics of the PJ–trough system and evidence for the development of the tropopause fold are presented in Section 3. Processes contributing to the formation of the fold are discussed in Section 4 in terms of an evaluation of the Sawyer (1956)–Eliassen (1962) circulation equation and a diagnostic evaluation of the ageostrophic winds and vertical motion near the polar jet streak. In Section 5, a literature review concerning the documentation of stratospheric extrusions and their possible role in cyclogenesis is presented, followed by Eulerian and Lagrangian diagnostics which are utilized to establish

a connection between the tropopause fold associated with the polar jet streak and the rapid cyclogenesis along the East Coast. Conservation of potential vorticity expressed in isentropic coordinates is used in Section 5 as a constraint from which to view cyclogenesis, and may be considered complementary to conventional, quasi-geostrophic diagnostic approaches framed in pressure coordinates, as has also been noted recently by Bleck and Mattocks (1984). The results of the analysis and possible implications of these findings are summarized in Section 6.

2. Analyses of surface data and satellite imagery

Bosart (1981) and Uccellini et al. (1984) present detailed synoptic overviews of the Presidents' Day cyclone. Therefore, only a brief summary of the surface analyses and a description of satellite imagery are presented here to 1) review the development of the cyclone, 2) identify the two distinct cloud masses which produced the heavy snow along the East Coast and 3) document the presence of very dry air extending downward to at least the 700 mb level immediately over the low pressure center during the period of rapid cyclogenesis, which is suggestive of the presence of stratospheric air in the vicinity of the developing cyclone.

The Presidents' Day cyclone developed when an inverted trough situated along the East Coast on 18 February 1979 rapidly evolved into a major snowstorm on 19 February 1979 (Fig. 1). At 00Z/18[1], snow and sleet were occurring over the southern United States (Fig. 1a), and by 12Z/18, moderate-to-heavy snow developed in the southeastern United States as an inverted trough extended northward from the Gulf of Mexico (Fig. 1b). At the same time, a separate area of heavy snow began to develop off the Southeast Coast in response to a combination of the increased divergence along the axis of a subtropical jet streak (STJ) (Uccellini et al., 1984) and also to the development of a coastal front (Bosart, 1981). By 00Z/19, weak surface lows formed along the coastal front–inverted trough near Georgia and at the northern extent of the inverted trough in the Ohio Valley (Fig. 1c). Heavy snow continued along the East Coast, while moderate-to-heavy snow developed in the Ohio Valley. By 12Z/19, cyclogenesis was in progress along the Virginia coast (Fig. 2d) with heavy snow falling at rates approaching 8 cm h^{-1} from Washington, DC northeastward toward New York City.

Our analysis in this paper concentrates on the rapid development phase of the Presidents' Day cyclone which occurred on 19 February. The explosive

---

[1] All times and dates for synoptic observations are expressed in the same format used by Uccellini et al. (1984).
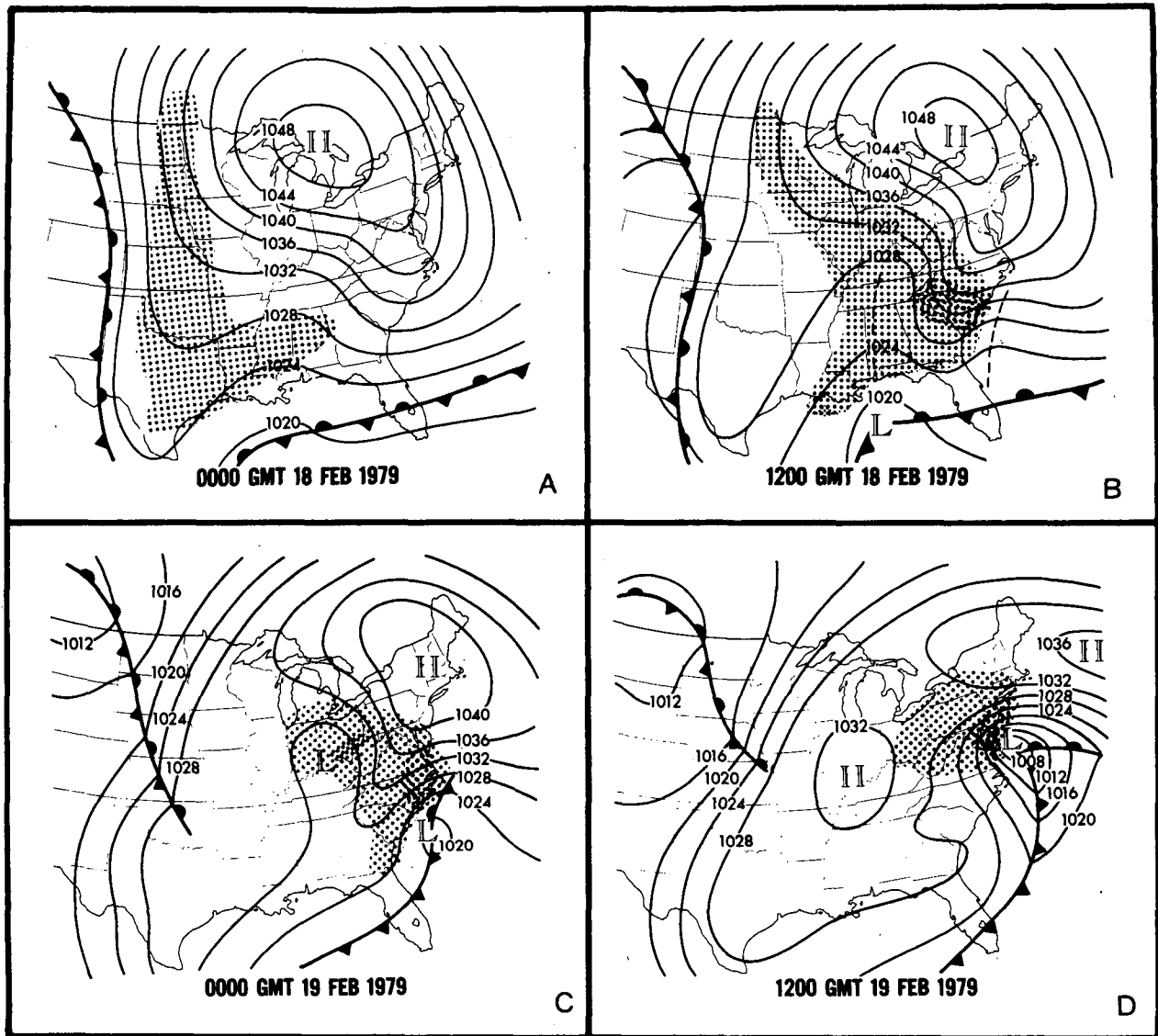
FIG. 1. Sea level pressure (mb) and surface frontal analyses for (a) 0000 GMT 18 February 1979; (b) 1200 GMT 18 February 1979; (c) 0000 GMT 19 February 1979; and (d) 1200 GMT 19 February 1979. Shading represents precipitation; dark shading indicates moderate-to-heavy precipitation. Dashed lines in (b) denote inverted and coastal troughs.

cyclogenesis and associated cloud distribution that yielded the heavy snowfall along the East Coast are depicted by the three-hourly SMS-GOES 11 μm infrared imagery (Fig. 2). The heavy snow on 18–19 February formed within two separate cloud masses that were respectively associated with the STJ and a polar jet streak (PJ) (Uccellini et al., 1984). At 06 Z/19 (Fig. 2a), the high clouds associated with the STJ (marked with an S) were located off the East Coast of the United States. The second cloud mass associated with the PJ–trough system (marked with P) was located over eastern Ohio and western Pennsylvania. A surface low was located off the North Carolina coast at the western edge of the cloud shield

associated with the STJ and had a central pressure of 1012 mb. At 09Z/19 (Fig. 2b), this surface low was positioned between the two cloud shields in an area of shallow (warmer) clouds and was deepening at a rate of 1 mb h⁻¹. The area of clouds associated with the STJ continued propagating eastward over the Atlantic Ocean and appeared to shrink in size. The clouds associated with the PJ–trough, to the north of the developing cyclone, propagated eastward, rapidly expanded in size and thickened (became colder) as an area of heavy snow moved from the Ohio Valley and intensified over the East Coast.

Between 12Z/19 and 15Z/19, explosive cyclogenesis commenced off the Virginia coast with the central
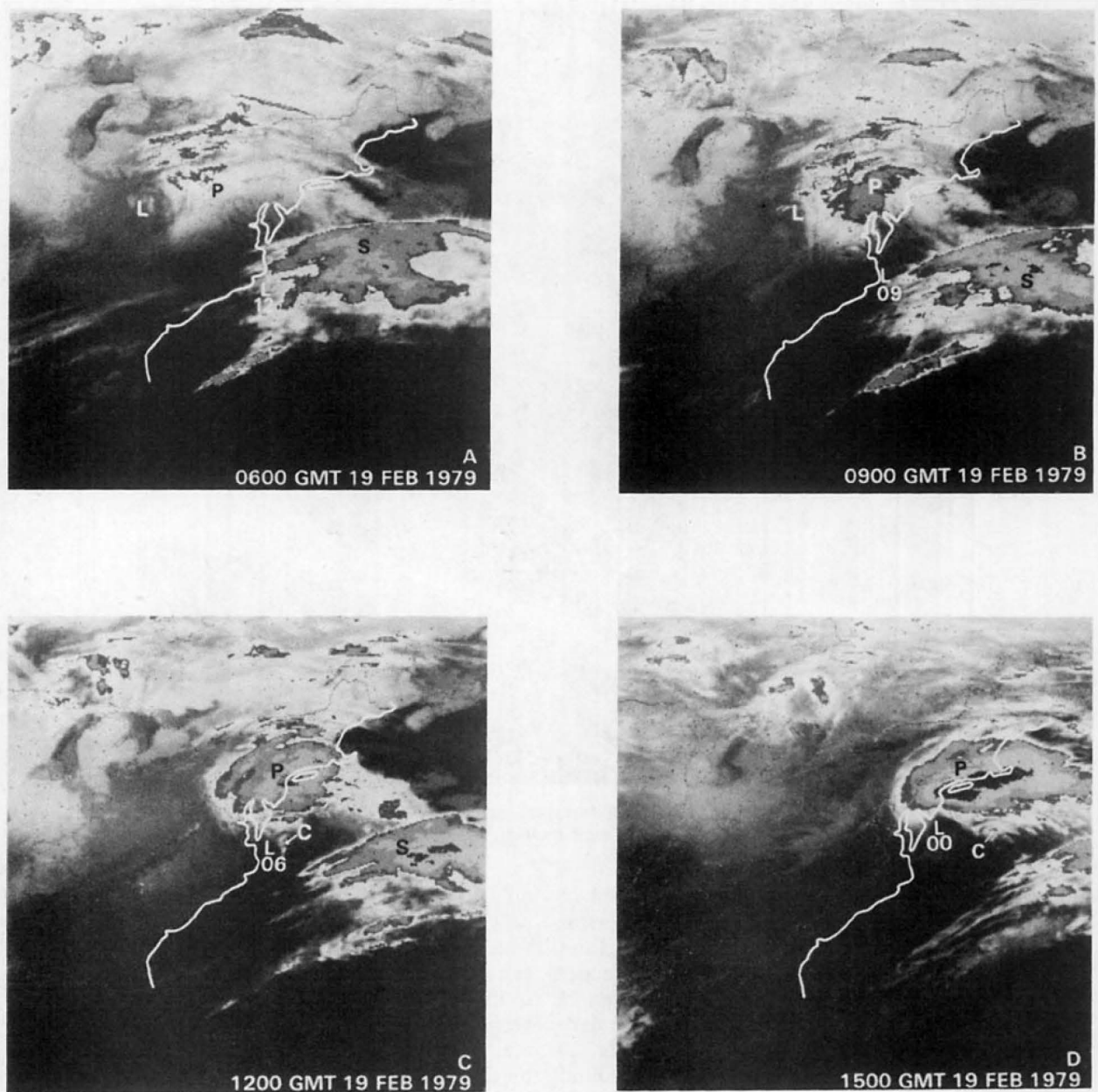
FIG. 2. Three hourly SMS-GOES infrared satellite imagery during cyclogenesis: (a) 0600 GMT 19 February 1979, (b) 0900 GMT 19 February 1979, (c) 1200 GMT 19 February 1979, and (d) 1500 GMT 19 February 1979. Visual remapping was performed for proper placement of East Coast map boundaries to correct operational misgridding of images; S and P represent positions of maximum winds associated with the subtropical and polar jet streaks, respectively, C represents position of convective cells to the east of the developing cyclone. The L represents surface lows with central pressures (mb; 06 is 1006 mb) listed for each time.

pressure decreasing at an average rate of 2 mb h^{-1} to 1000 mb (Fig. 2d) in an area that continued to be free of deep (cold) clouds, between the shrinking cloud mass associated with the STJ and the rapidly expanding cloud mass associated with the PJ–trough system. The band of isolated convective cells, marked with a C in Figs. 2c and 2d, was positioned to the east of the cyclone center at 12Z/19 (Fig. 2c), but propagated rapidly away from the center of the storm

by 15Z/19 (Fig. 2d). Bosart (1981) places particular emphasis on this line of convection as one which possibly played an important role in the rapid intensification of the cyclone.

By 18Z/19, the storm was rapidly evolving into a major vortex as the central pressure fell 10 mb in 3 h to 990 mb and an eye-like, cloud-free area developed near the storm center (Fig. 3). The SMS-GOES visible image at 1830Z/19 shows that the cyclone vortex
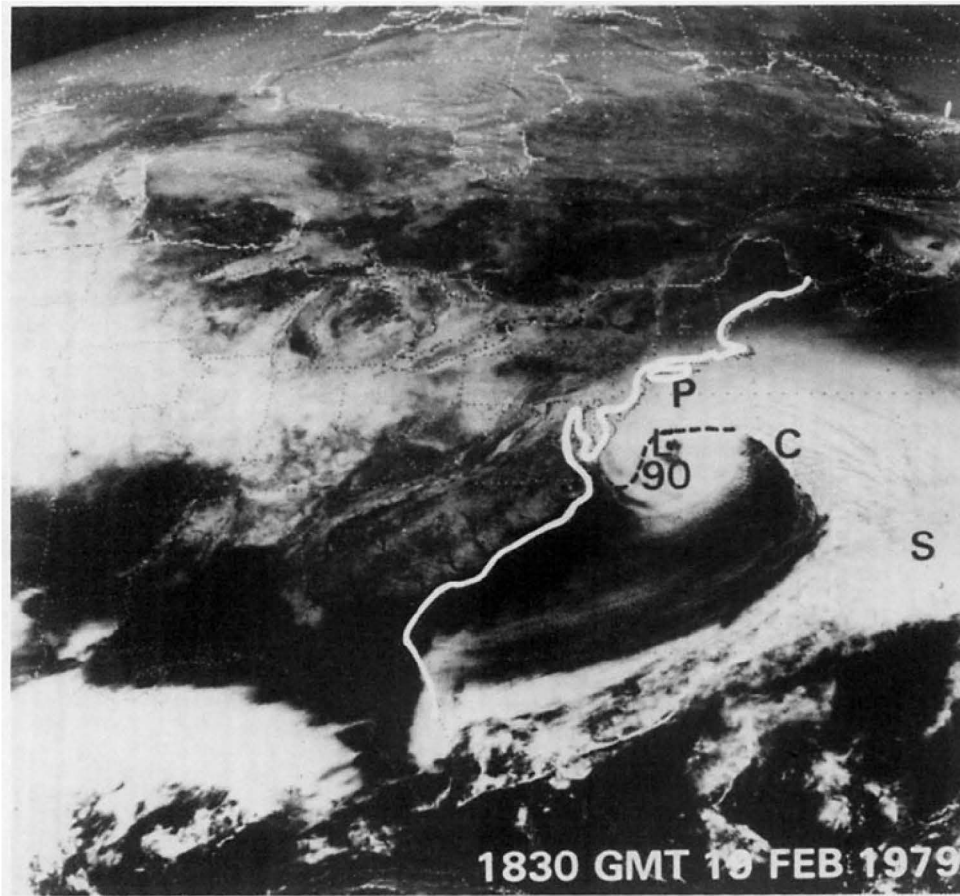
FIG. 3. SMS-GOES visible satellite imagery for 1830 GMT 19 February 1979.
Labels have same meaning as in Fig. 2.

maintained a noticeably asymmetric distribution of clouds that was also evident in the infrared images at 12Z/19 and 15Z/19 (Figs. 2c and 2d). The cloud distribution was marked by 1) higher and deeper cloud cover and imbedded convection extending in an east–west direction with a sharp southern boundary situated immediately north of the storm center, 2) the middle- and upper-level clouds wrapping around the storm center in the northwest quadrant, and 3) low stratus clouds around the storm center and to its south and east. The convective clouds that developed near the storm center around 12Z/19 (Fig. 2c) have moved to a position farther to the east of the cyclone center, ahead of the clear tongue in the southeastern quadrant of the storm.

The 11 μm infrared images indicate that the cyclone developed rapidly after 12Z/19 and was centered in a region generally free of deep clouds. Moisture imagery from the 6.7 μm channel on the Tempera-ture–Humidity Infrared Radiometer (THIR) instru-ment aboard the Nimbus 7 polar-orbiting satellite confirm that very dry air was located over and to the south of the center of the rapidly developing cyclone

on 19 February (Fig. 4b). As described by Rodgers et al. (1976), the 6.7 μm band on the THIR measures water vapor in the middle to upper troposphere, generally between 300 and 500 mb, and can be used to infer dynamical processes, moisture advection and vertical motion patterns associated with synoptic-scale systems. Since the amount of radiation received by the satellite in the 6.7 μm band is a function of both water vapor content and temperature, it is difficult to define the precise altitude of water vapor signals measured in this infrared band. However, the interpretation of the satellite 6.7 μm image is unam-biguous for dry regions since the warm low-level temperature observed through the dry midlevel air will provide a distinct and sharply contrasting signal to any surrounding midlevel moisture (Petersen et al., 1984). Additionally, for dry upper-tropospheric conditions, the level of maximum radiance for the 6.7 μm channel shifts significantly downward in height. Thus, pronounced dry (warm) signatures on the imagery represent dry conditions not only near the 400 mb level, but throughout a deep layer of the atmosphere extending downward to 700 mb.
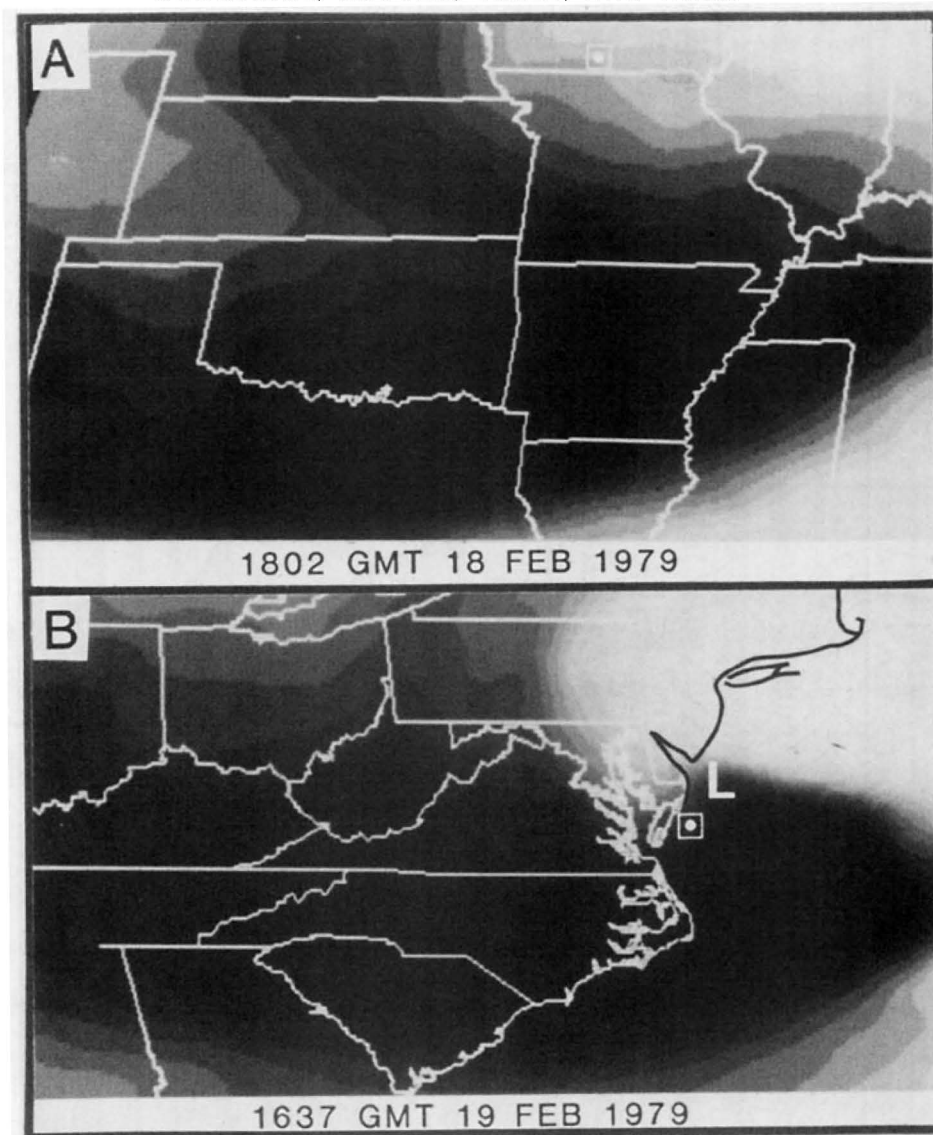
FIG. 4. Water vapor infrared imagery from the Temperature–Humidity Infrared Radiometer (THIR) on Nimbus 7 for (a) 1802 GMT 18 February 1979 and (b) 1637 GMT 19 February 1979. Gray scale for 1637 GMT (b) 1.4 W m^{-2} sr^{-1} in driest air (darkest gray shade) south of cyclone, 1.2 W m^{-2} sr^{-1} in dry slot near L, and 0.3 W m^{-2} sr^{-1} in cloud regime north of cyclone center. Similar scale used for (a). Boxes in (a) and (b) indicate positions of ozone maximum measured by the Total Ozone Mapping Spectrometer (TOMS); see Fig. 11 for TOMS analysis. The L in (b) indicates estimated position of surface low for 1500 GMT.

For this case, the 6.7 μm THIR imagery for 18 and 19 February indicate that intersecting bands of very dry air were located over the central United States on 18 February, a pattern which is characteristic of merging polar and subtropical jet streaks (Petersen *et al.*, 1984). At 1802 GMT 18 February, a band of dry air was directed from Nebraska toward southern Missouri (Fig. 4a) along the axis of the PJ (Figs. 5b1 and 5c1). Another band of dry air was located from northeastern Texas to western Tennessee within the

confluent entrance region of the STJ (see Fig. 4a1 in Uccellini *et al.*, 1984). These separate dryness bands appear to have combined into one major dry region by 1637 GMT 19 February, extending across the Middle Atlantic states to a position approximately 500 km off the East Coast (Fig. 4b). The 700 mb analyses (not shown) indicate that between 12Z/18 and 12Z/19 an expanding area of very dry air coincided with the northern dry slot on the THIR image at 18Z/18 (Fig. 4a). The dry region at 700 mb reached
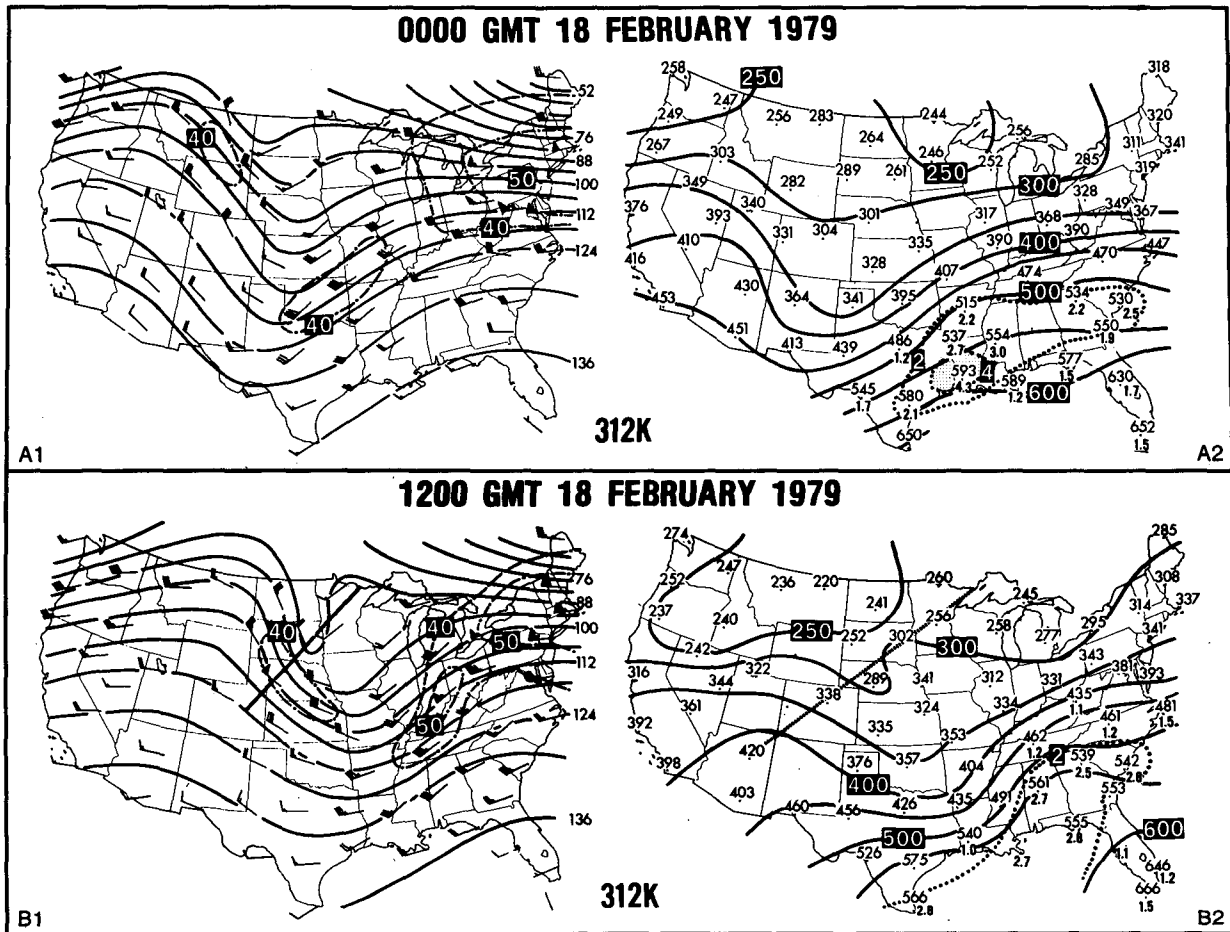
FIG. 5. Isentropic analyses for 312 K surface for (a) 0000 GMT 18 February 1979; (b) 1200 GMT 18 February 1979; (c) 0000 GMT 19 February 1979; (d) 1200 GMT 19 February 1979. For (a1)–(d1), Montgomery streamfunction analysis (solid, 100 = 3.100 × 10^5 m^2 s^{-2}) and isotachs (dot dashed, m s^{-1}). Wind barbs represent observed speeds (whole barbs denote 10 m s^{-1}; half barbs denote 5 m s^{-1}). For (a2)–(d2), pressure (solid, mb) and mixing ratio (dotted, g kg^{-1}). Shading represents mixing ratio greater than 4 g kg^{-1}. Solid lines in (b1) and (c1) indicate positions of cross sections in Figs. 9 and 10, respectively; dashed line in (b2) indicates position of cross sections in Figs. 12–14.

the North Carolina-Virginia coast by 12Z/19, again coinciding with the dry signal in the THIR image (Fig. 4b). The THIR 6.7 μm image for 19 February also shows that the surface low pressure system appears to be developing within a well-defined notch in the dry air just east of the Delmarva Peninsula, indicating that very dry air was extending downward to at least the 700 mb level immediately above the rapidly developing vortex depicted in the visible image (Fig. 3), and more generally to its south and east.

3. Evidence for the amplifying PJ–trough system and associated tropopause fold preceding rapid cyclogenesis

In this section, radiosonde and total ozone analyses are presented that focus on the tropopause fold that

appeared prior to the development of the Presidents' Day cyclone. As with the Uccellini et al. (1984) study, the radiosonde analyses used for the diagnostics in Sections 4 and 5 were generated by an objective isentropic analysis scheme developed by Petersen (1979). Wind, moisture, and pressure analyses were derived on a 2 by 2° latitude–longitude grid for isentropic surfaces extending from 264 to 380 K at a 4 K increment. The 312 K surface is shown in Fig. 5, since this surface passes through a layer within which the PJ propagated toward the East Coast and intensified between 00Z/18 and 12Z/19. The total ozone analysis was obtained from the TOMS aboard Nimbus 7.

a. Radiosonde analyses

At 00Z/18 the 312 K analyses show the PJ to be located near a ridge crest and propagating southeast-
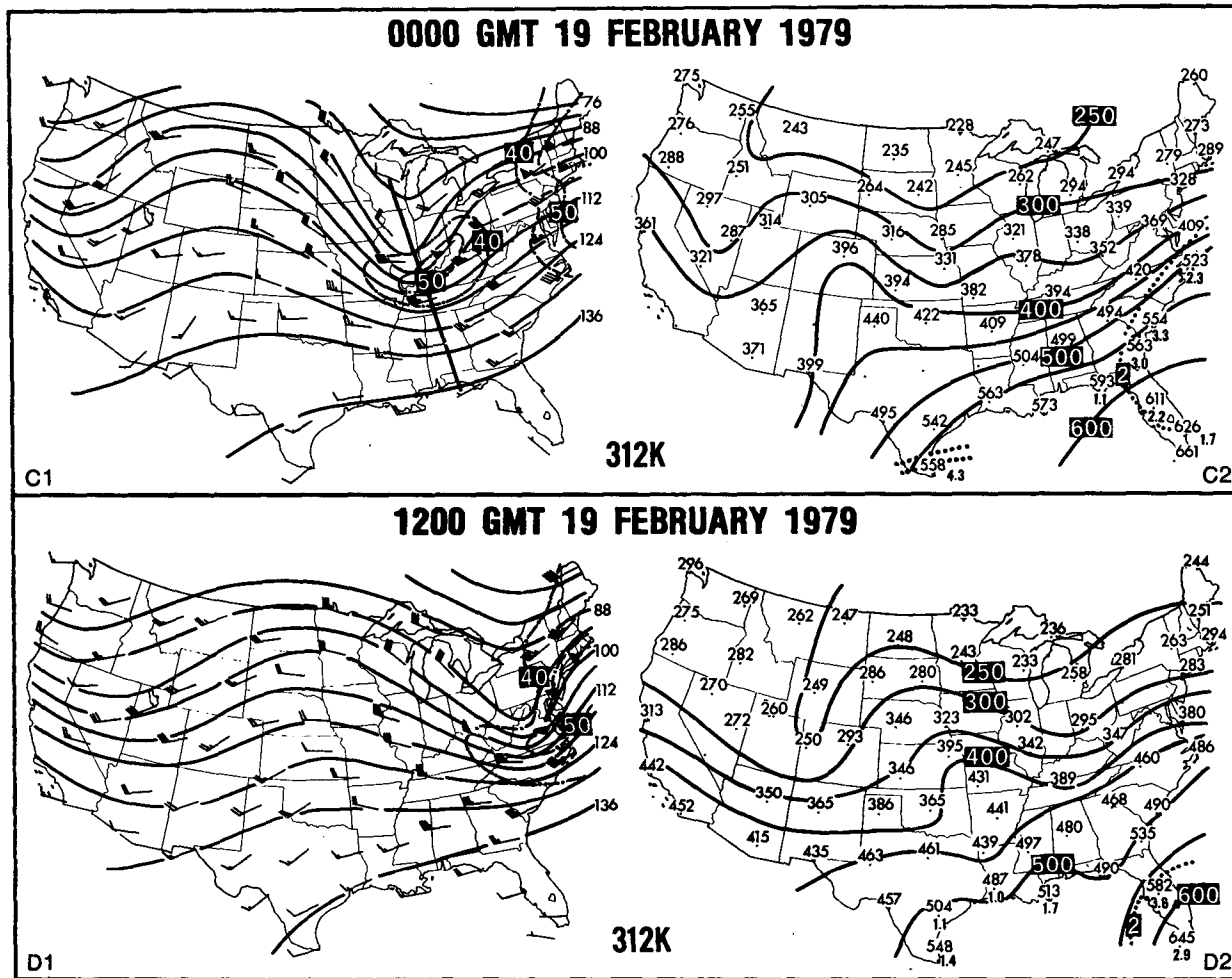
FIG. 5. (*Continued*)

ward across Montana between 250 and 300 mb (Figs. 5a1 and 5a2). By 12Z/18 the PJ was situated midway between the ridge and trough axes, extending downward from 250 to around 330 mb (Figs. 5b1 and 5b2). By 00Z/19 the PJ had intensified to greater than 50 m s^{-1}, reached the base of the trough, and descended to 400 mb (Figs. 5c1 and 5c2). Between 00Z/18 and 00Z/19, the trough associated with the PJ also amplified, as both the magnitude of the gradients of the Montgomery streamfunction (ψ_m) and the curvature near its base increased (Figs. 5b1 and 5c1). The PJ-trough system was located upstream of the heavy snow that developed in the Ohio Valley by 00Z/19 (Fig. 1c). By 12Z/19, the PJ-trough system propagated to the East Coast without noticeable amplification detected in either the jet streak or the trough (Fig. 5d1). Cyclogenesis began offshore near this time and the cloud mass in the exit region of the PJ rapidly expanded over the Middle Atlantic states (Fig. 2c).

Areal-averaged profiles of adiabatic mass flux divergence and vertical motion (ω) are presented in Figs. 6, 7 and 8 for 12Z/18, 00Z/19 and 12Z/19, respectively, to depict the general structure and evolution of the PJ-trough system as it propagated from the central United States and merged with the coastal system located immediately off the East Coast. The adiabatic mass flux divergence is computed in the isentropic framework using the expression $\nabla_\theta \cdot (\partial p/\partial \theta \mathbf{U})$, where $\partial p/\partial \theta$ is the inverse static stability and a measure of mass in isentropic coordinates and U is the total wind. The mass flux divergence term is not only a measure of the adiabatic mass adjustment within an isentropic layer, but is also related directly to changes in the static stability, as discussed in Section 5b. The vertical motion is computed from the continuity equation in pressure coordinates, using the O'Brien (1970) correction scheme as discussed by Uccellini *et al.* (1984). There are three areas represented in the map insets in Figs. 6
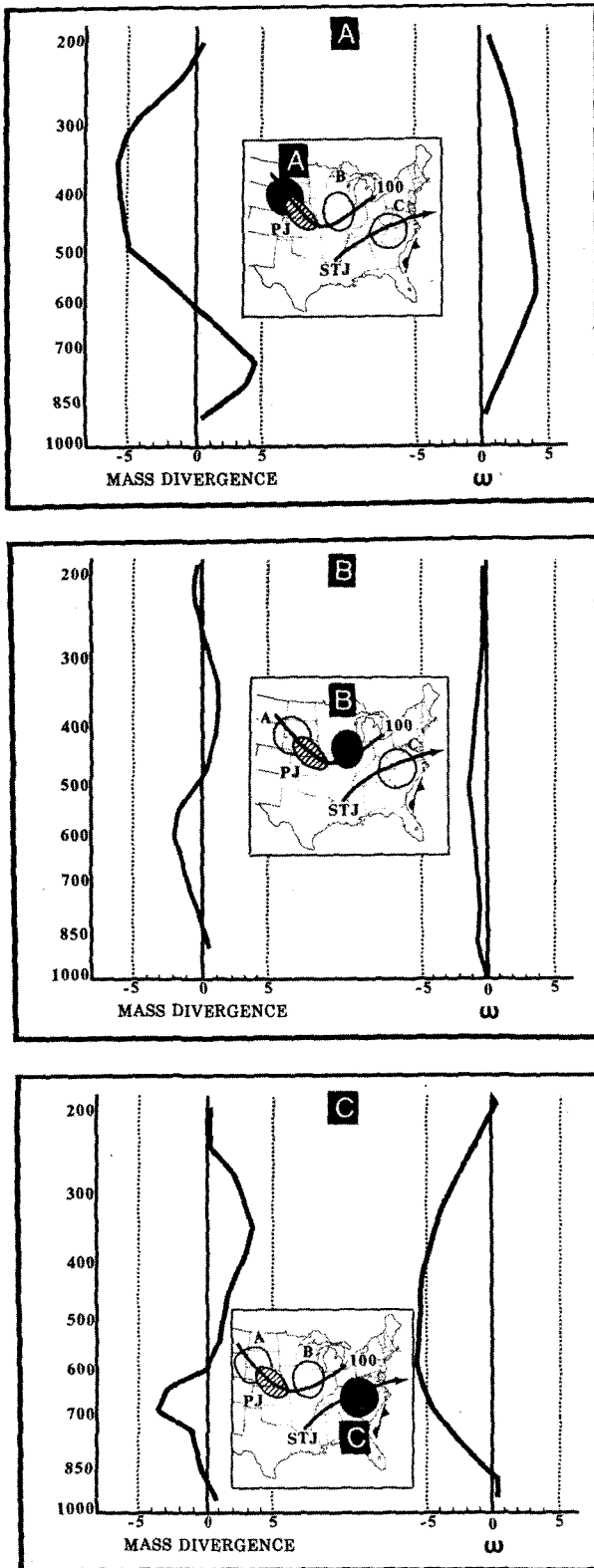
and 7 for which the spatial averages were computed at 12Z/18 and 00Z/19, including 1) the area upstream of the trough axis in the entrance region of the PJ, 2) the area downstream of the trough axis in the exit region of the PJ, colocated with the area of clouds as determined by the satellite imagery and 3) the area immediately west of the coastal front near the axis of the STJ, as analyzed by Uccellini et al. (1984). At 12Z/19, only the areal-averaged profiles on either side of the trough axis were computed (Fig. 8) since the PJ–trough and coastal front systems seemed to have merged by this time.

As the PJ propagated toward the base of the amplifying trough at 12Z/18, the region upstream of the trough axis was already marked by a well-defined two-layer mass divergence profile (Fig. 6a), with mass convergence maximized between 500 and 300 mb and mass divergence maximized near 750 mb. Strong descent was also diagnosed throughout the troposphere with the maximum sinking motion greater than 3.5 μb s^{-1} diagnosed between 450 and 650 mb. The strong descent corresponds with the northern dry band in the 6.7 μm THIR image at 18Z/18 (Fig. 4a). In contrast to the entrance region of the PJ, the area downstream of the trough axis was characterized by mass divergence and vertical motion profiles that were not well defined. At 12Z/18, weak upper-level (lower-level) mass divergence (convergence) and a weak ascent pattern were diagnosed (Fig. 6b), which corresponded with the light snow over the north-central United States (Fig. 1b). West of the coastal front and near the axis of the STJ, a distinct two-layer mass divergence profile and a deep layer of strong ascent, with minimum ω values exceeding -5 μb s^{-1}, was evident at 12Z/18 (Fig. 6c) in the region marked by heavy snow (Fig. 1b). Uccellini et al. (1983, 1984) have linked this vertical motion to a combination of the temporally increasing divergence along the axis of the STJ and diabatic processes along the Southeast Coast.

As the PJ–trough system amplified between 12Z/18 and 00Z/19, the area upstream of the trough axis at 00Z/19 was marked by the same general two-layered mass divergence pattern and strong descent throughout the entire troposphere (Fig. 7a) as before, although the level of maximum mass convergence had shifted downward toward the 500 mb level in conjunction with the descending and amplifying PJ (Figs. 5b and 5c). However, downstream of the trough axis, the two-layered mass divergence profile had become better defined by 00Z/19 (Fig. 7b), with mass

FIG. 6. Areal-averaged profiles of the adiabatic mass divergence (5 = 5 × 10^{-5} mb K^{-1} s^{-1}) and vertical motion (μb s^{-1}) for 1200 GMT 18 February 1979 (the vertical coordinate is ln$p$). The profiles are computed for the lettered areas shaded in the map inserts for each set in (a), (b) and (c). The map inserts contain the position of

the trough on the 312 K surface indicated by the Montgomery streamfunction (ψ_m) contour (100 = 3.100 × 10^5 m^2 s^{-2}), the location of the polar jet on the 312 K surface indicated by hatched region (denoting wind speeds greater than 40 m s^{-1}), the position of the subtropical jet axis on the 332 K surface indicated by the extended arrow labeled STJ (from 332 K analyses in Uccellini et al., 1984), and the position of the coastal front.

divergence increasing above the 700 mb level and exceeding 3×10^{-5} mb K^{-1} s^{-1} between 650 and 500 mb. The upward vertical motion also increased, with the maximum ascent of -3 μb s^{-1} located between
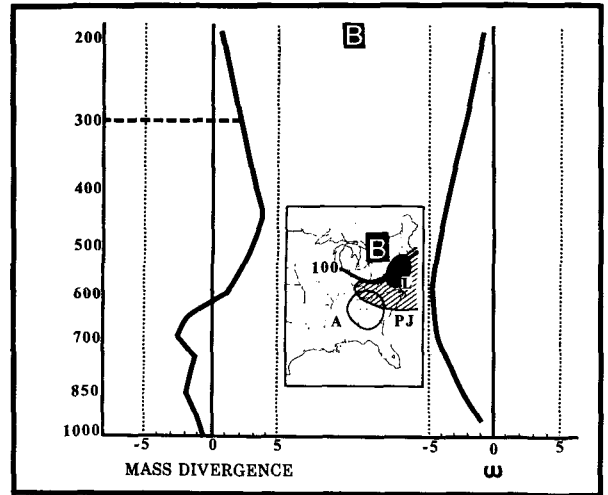
FIG. 8. Areal-averaged profiles of the adiabatic mass divergence and vertical motion for 1200 GMT 19 February 1979. See Figs. 6 and 7 for details. Dashed line on mass divergence profile indicates mass convergence was diagnosed in a very shallow isentropic layer near the 300 mb level.

850 and 650 mb, which is consistent with the development of moderate snow in the Ohio Valley by 00Z/19 (Fig. 1c) and the expanding cloud shield as depicted by the infrared imagery after 06Z/19 in Fig. 2 (see also Fig. 2c and 2d in Uccellini et al., 1984). The mass divergence and vertical motion profiles for the area to the west of the slowly developing surface low and coastal front (Fig. 7c) show the same general pattern as before.

By 12Z/19, the PJ–trough system moving from the central United States had essentially overtaken the coastal system, with the rapid cyclogenesis commencing off the East Coast (Fig. 1d). In the region upstream
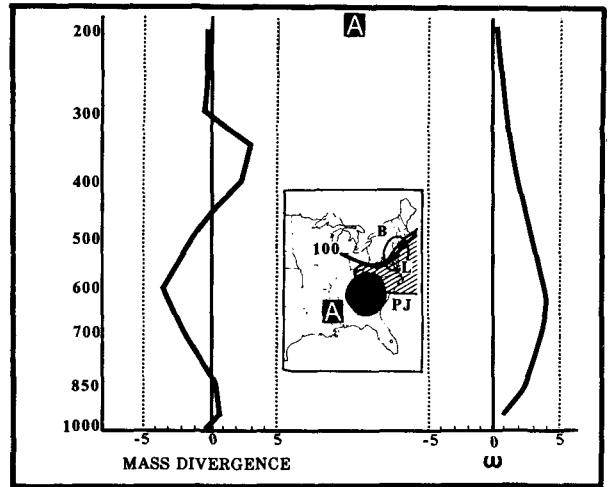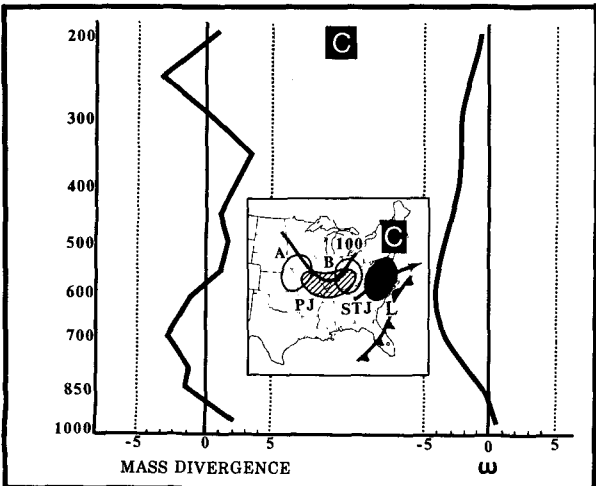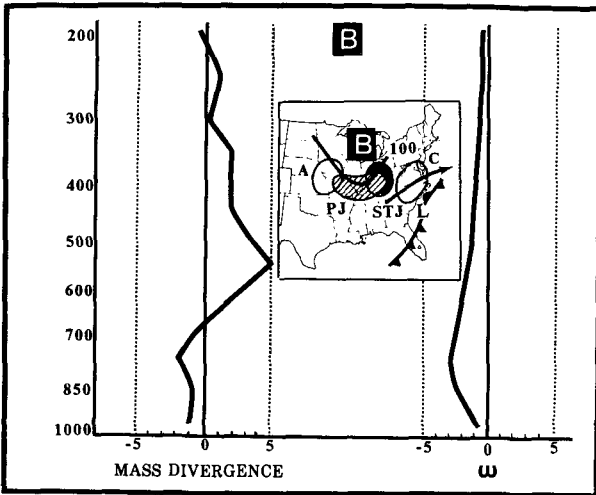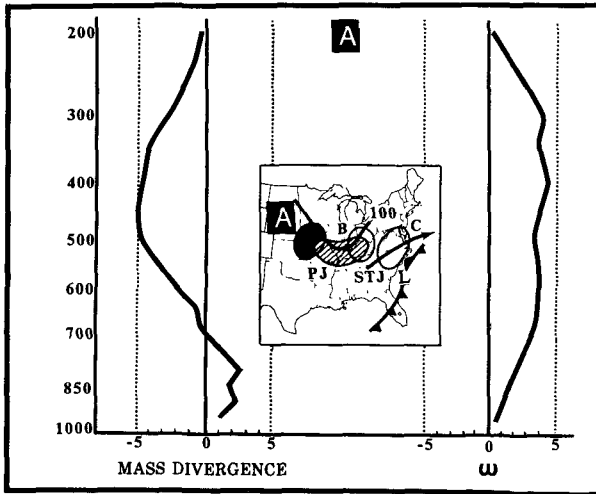
FIG. 7. Areal-averaged profiles of the adiabatic mass divergence and vertical motion for 0000 GMT 19 February 1979. Details as in Fig. 6 except cyclone position along coast included.

of the trough axis, the mass divergence profile no longer displayed the distinct two-layer structure as before, as the area of largest mass convergence continued to shift to higher pressure (near the 600 mb level) in conjunction with the descending PJ. Nevertheless, descent was still diagnosed throughout the entire troposphere (Fig. 8a), which corresponds well with the dry band observed by the 6.7 μm THIR channel (Fig. 4b). The areal extent and orientation of the region downstream of the trough axis and north of the developing cyclone are constricted because of data limitations off the East Coast. Even with the restricted data set, the mass divergence and vertical motion profile indicate that the merger of the PJ-trough and coastal front systems resulted in significant changes in the downstream portion of the PJ-trough system between 00Z/19 and 12Z/19 (Fig. 8b) that include: 1) a deeper layer of mass convergence of increased magnitude extending from the surface up to 625 mb; 2) mass divergence above 625 mb with maximum values still exceeding 3×10^{-5} mb K^{-1} s^{-1} between 625 and 450 mb; and 3) increasing upward vertical motion throughout the entire troposphere, with ω exceeding -4 μb s^{-1} between 725 and 450 mb. Our diagnosis of increasing ascent downstream of the trough axis, as it propagated eastward and appeared to merge with the coastal system between 00Z/19 and 12Z/19, agrees with Bosart and Lin's (1984) semigeostrophic analysis and corresponds with the explosively expanding cloud mass (Fig. 2d) and heavy snowfall (Fig. 1d) in the Middle Atlantic states by 12Z/19.

The intensification of the PJ-trough system between 12Z/18 and 00Z/19 was marked by strong descent upstream of the trough axis which preceded the development of a coherent ascent pattern, an expanding cloud shield, and the increasing intensity of snowfall in the Ohio Valley. This finding is consistent with the well-known synoptic-scale distribution of vertical motion associated with amplifying wave systems (Krishnamurti, 1968). Vertical cross sections constructed across the axis of the PJ at 12Z/18 and 00Z/19 are now presented to provide supporting evidence that the region of strong descent in the central United States was concentrated within a tropopause fold[2] along the axis of the PJ. The cross sections (Figs. 9 and 10) include isentropes, geostrophic wind speeds computed using the Whittaker and Petersen (1977) scheme, total wind speeds subjectively analyzed within the plane of the cross section, and potential vorticity. The potential vorticity was computed on a three-dimensional array of grid points using the expression,

---

[2] A tropopause fold is defined by Reed (1955) and Reed and Danielsen (1959) as an extrusion of stratospheric air within an upper-tropospheric baroclinic zone which slopes downward from a normal tropopause level to the middle troposphere (500 to 700 mb).

$-(\zeta_\theta + f)\partial\theta/\partial p$, where ζ_θ is the relative vorticity measured on isentropic surfaces, f is the Coriolis parameter, θ is potential temperature, and p is pressure. The potential vorticity was bilinearly interpolated to the plane of the cross sections.

The cross section at 12Z/18 extends from International Falls, Minnesota (INL) to Denver, Colorado (DEN) (see solid line in Fig. 5b1) and shows that the core of the PJ was located just above the 300 mb level near North Platte, Nebraska (LBF). The vertical wind shears beneath the jet were spread over the layer between 800 and 400 mb (Fig. 9a) within a frontal zone extending downward from 300 mb at Huron, South Dakota (HON) to 650 mb at LBF. Stratospheric values of potential vorticity, defined as those values greater than 10×10^{-6} K mb^{-1} s^{-1} by Reed and Danielsen (1959) and Shapiro (1976), extend downward within the weak front to near the 500 mb level on the cyclonic side of the jet axis (Fig. 9b).

The vertical cross section at 00Z/19 along the line from Green Bay, Wisconsin (GRB) to Apalachicola, Florida (AQQ) (see solid line in Fig. 5c1) depicts the STJ core near 200 mb near Centreville, Alabama (CKL) and the PJ located between Salem, Illinois (SLO) and Nashville, Tennessee (BNA). The intensification of the PJ between 12Z/18 and 00Z/19 is represented in Figs. 10a and 10b by an increase in the observed and geostrophic wind maxima to 55 and 60 m s^{-1}, respectively, and an increase in the vertical wind shear. By 00Z/19, the vertical wind shear was concentrated in the 500 to 700 mb layer within a well-defined front extending beneath the PJ from 550 mb at SLO to 700 mb at BNA (Fig. 10b). A further indication of the intensification of the PJ-trough system between 12Z/18 and 00Z/19 is the downward extension of high values of potential vorticity to the 700 mb level within the frontal zone between SLO and BNA, resembling the structures analyzed, for example, by Reed and Danielsen (1959) and Shapiro (1976). Given the rather coarse resolution of the operational data base compared to research data sets obtained from aircraft (e.g., Shapiro, 1976; Danielsen and Mohnen, 1977), it is likely that the diagnosed values of potential vorticity computed on a $2 \times 2°$ grid underestimate the actual values. Nevertheless, the cross section analyses indicate that by 00Z/19, a tropopause fold has developed within the region of strong upper-level mass convergence and descent that was diagnosed between the trough axis and upstream ridge as the PJ-trough system propagated toward the Ohio Valley.

b. Ozone analysis

Large concentrations of ozone measured by instrumented aircraft have been used as another indication of stratospheric air within a folded tropopause (Shapiro, 1978, 1980; Danielsen and Mohnen, 1977;
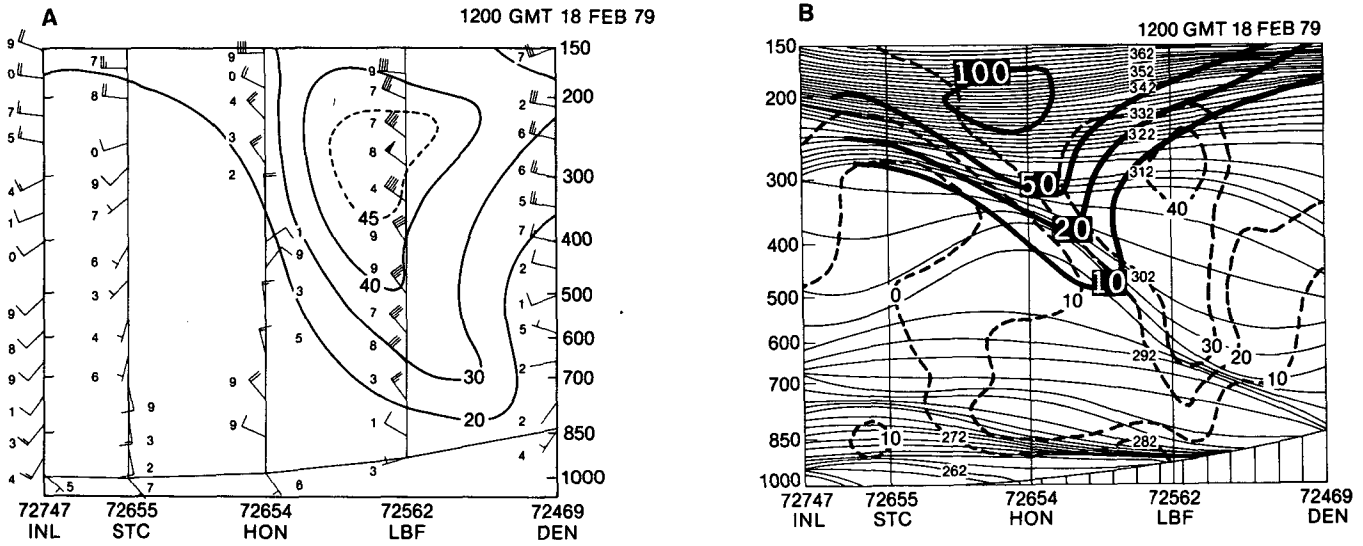
FIG. 9. Vertical cross section from International Falls, Minnesota (INL) to Denver, Colorado (DEN) for 1200 GMT 18 February 1979. (a) Isotach analysis for total wind speed (solid, m s^{-1}). Wind barbs plotted with last digit of wind observation. (b) Isentropes (solid, K), geostrophic wind (dashed, m s^{-1}) computed from the horizontal thermal gradient in the plane of cross section, and potential vorticity, $-(\zeta_\theta + f)(\partial\theta/\partial p)$, heavy solid where $10 = 10 \times 10^{-6}$ K mb^{-1} s^{-1}. Potential vorticity analysis only shown for upper portion of frontal zone and stratosphere.

Danielsen, 1980). Ozone measurements from instrumented aircraft have also been used to infer the presence of dry stratospheric air near the center of the region of cyclogenesis in the Gulf of Genova on 24–25 April 1982 during the Alpine Experiment (ALPEX) in Europe (Buzzi et al., 1984). For our study of the Presidents' Day storm, ozone concentrations observed by the TOMS are used to provide supporting evidence for the existence of the tropopause fold on 18 February. Shapiro et al. (1982) and Schoeberl and Krueger (1983) provide details on the

TOMS instrument flown aboard the Nimbus 7 satellite. Bhartia et al. (1984a, 1984b) have determined that TOMS has a slight bias (−4%), compared with total ozone measurements from balloons, rockets and ground-based measuring systems, that is easily correctable and of little consequence to studies of the dynamical processes involving ozone. Shapiro et al. (1982) compared TOMS and aircraft measurements and found TOMS to be a useful observing system for locating tropopause folds.

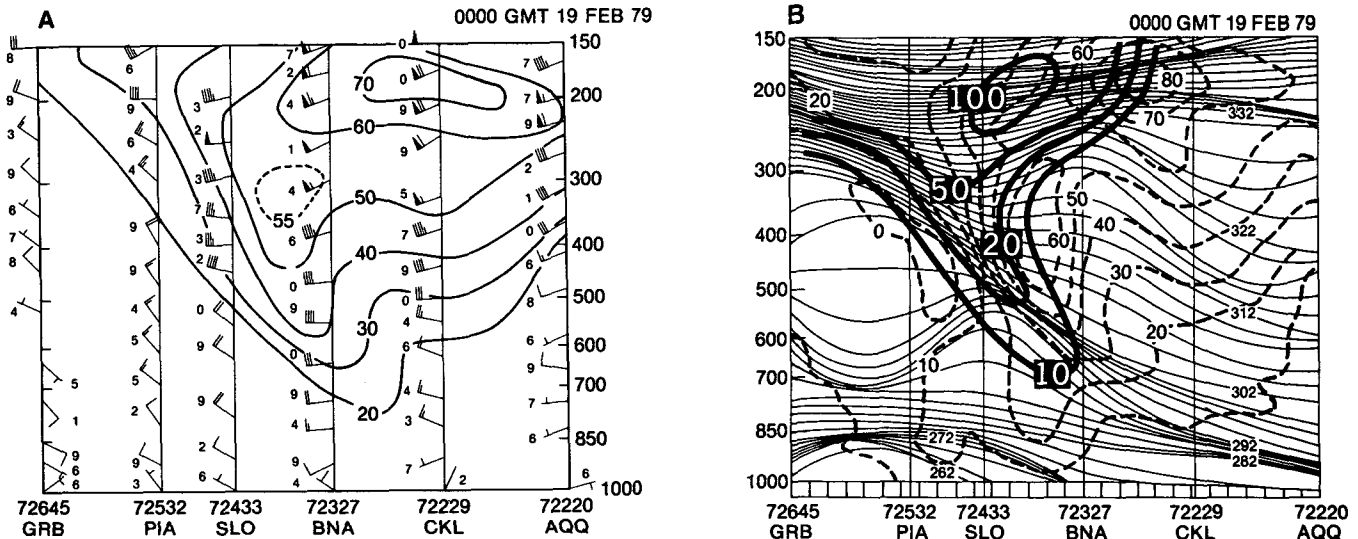The ozone distribution measured by TOMS is

FIG. 10. As in Fig. 9 except from Green Bay, Wisconsin (GRB) to Apalachicola, Florida (AQQ) for 0000 GMT 19 February 1979.
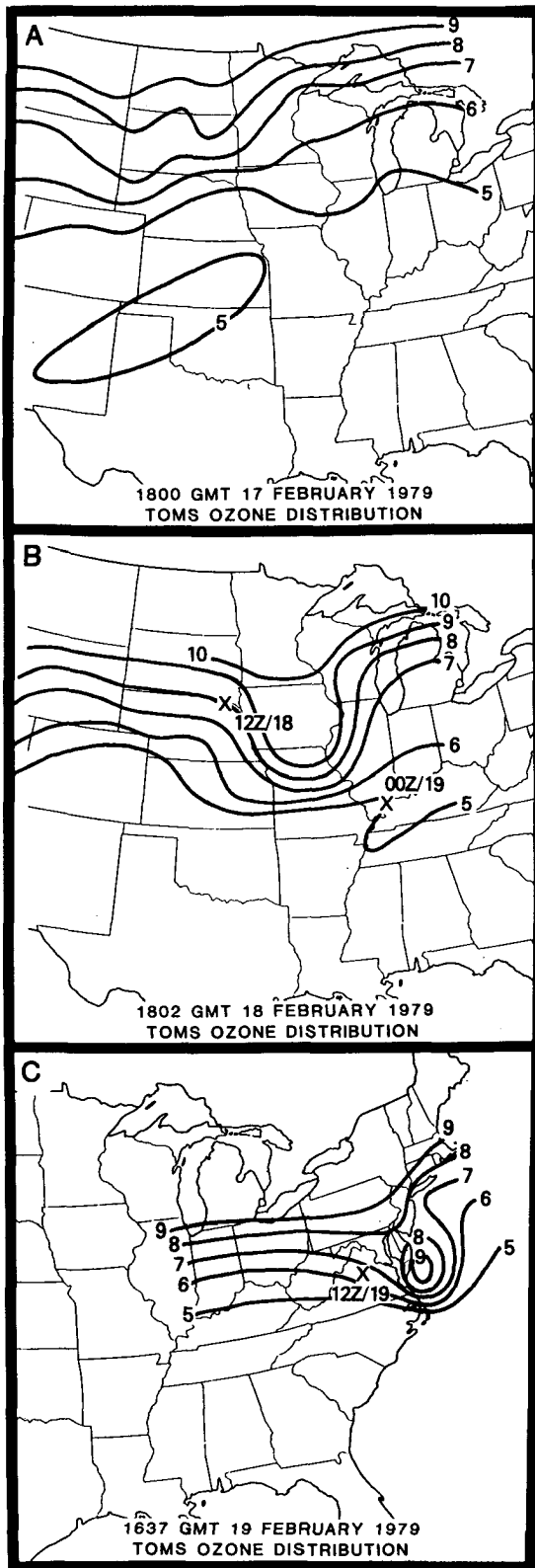
FIG. 11. Total ozone distribution as measured by the Total Ozone Mapping Spectrometer (TOMS) aboard the Nimbus 7 polar-

positively correlated with the depth of the stratosphere in that maximum ozone concentrations indicate a relatively thick stratosphere and a correspondingly thinner troposphere. Since TOMS is on a polar-orbiting satellite and measures reflected ultraviolet solar radiation, the ozone information is available only once each day at an asynoptic time. Nevertheless, the sequence of daily images derived from the TOMS instrument from 17 February to 19 February 1979 (Fig. 11) illustrates that a significant change occurred in the ozone distribution where the tropopause fold developed. At 1800 GMT 17 February, no distinct features in the ozone analysis are discernible (Fig. 11a). (An analysis of the TOMS data from the next overpass across the West Coast does not show any noticeable modulation of maximum ozone associated with the PJ at this time.) However, by 1802 GMT 18 February, a large modulation in the ozone field is evident with the north–south axis of maximum ozone (in the range of 385 to 400 Dobson units; between the 9 and 10 contours in Fig. 11b) in Iowa located upstream of the cross section analysis of the tropopause fold at 00Z/19 (Fig. 10). By 1637 GMT 19 February, the pronounced ozone maximum had moved to a position located along the East Coast (Fig. 11c). The TOMS data on 19 February 1979 indicate that the deep stratospheric air mass which first appeared in the central United States on 18 February was located close to the center of the developing low, as observed by the SMS-GOES infrared image (Fig. 2d).

In summary, the radiosonde analysis indicates the trough amplification was maximized in the central United States between 12Z/18 and 00Z/19, 12 to 24 h prior to the rapid cyclogenesis off the East Coast. The temporal evolution of the PJ–trough system and associated thermal field for this case is very similar to the "asymmetrical" structure of amplifying upper-level troughs preceding low-level cyclogenesis discussed by Krishnamurti (1968) and Palmén and Newton (1969, see pp. 335–338). Furthermore, upper-level frontogenesis and a deep tropopause fold could be diagnosed in a well-defined area of descent between the trough axis and upstream ridge prior to the increase in ascent and associated expansion of the cloud mass downstream of the trough axis that occurred between 00Z/19 and 12Z/19 as the trough propagated toward the East Coast. In the following

section, the Sawyer–Eliassen equation is used to diagnose the processes contributing to the subsidence which produced the tropopause fold over the central United States. Diagnostic analyses are then presented in Section 5 relating the stratospheric extrusion to the subsequent cyclogenesis along the East Coast.

4. Diagnosis of the vertical circulation associated with the incipient tropopause fold

The results of numerous case studies of upper-level frontogenesis and tropopause folding (e.g., Reed and Sanders, 1953; Newton, 1954; Reed, 1955; Reed and Danielsen, 1959; Danielsen, 1964, 1968; Bosart, 1970; Shapiro, 1970) and numerical modeling and theoretical studies (e.g., Mudrick, 1974; Shapiro, 1975; Heckley and Hoskins, 1982; Newton and Trevisan, 1984a, 1984b) have established that these associated processes are a consequence of subsidence that is maximized within and to the warm side of the developing frontal zone. In this section, the diagnostic ageostrophic circulation equation of Sawyer (1956) and Eliassen (1962) will be utilized to obtain patterns of vertical motion compatible with the results of the above studies for the initial stages of the tropopause folding process on 12Z/18 shown in Fig. 9.

The vertical cross section for which the ageostrophic stream function is to be determined extends along a rhumb line from extreme northeastern Minnesota (48°N, 90°W) to northeastern Arizona (36°N, 110°W) (see Fig. 5b2: note proximity to the cross section in Fig. 9). This cross section cuts across the core of the polar jet streak situated approximately within the inflection in the ψ_m field (Fig. 5b1). The PJ was also situated in a region of cold advection in the northwesterly flow (Fig. 5b2) upstream of the intensifying shortwave trough, a configuration that has been identified by Shapiro (1982) as particularly favorable for upper-level frontogenesis (see Shapiro's Fig. 7b).

The version of the Sawyer–Eliassen equation used for the vertical circulation diagnosis is cast in terms of the so-called pseudo-height introduced by Hoskins and Bretherton (1972), defined as

$$z = z_a \left[1 - \left(\frac{p}{p_0} \right)^{R/c_p} \right], \qquad (1)$$

where $z_a \ (=c_p\theta_0/g)$ is a reference height, p is pressure, $p_0 \ (=1000 \ \text{mb})$ is a reference pressure, R is the ideal gas constant for dry air, c_p is the specific heat of dry air at constant pressure, θ_0 is a reference potential temperature and g is gravity. The Sawyer–Eliassen equation for the stream function, ψ, for the ageostrophic flow in the x–z plane for *adiabatic, frictionless conditions* is

$$-N^2 \frac{\partial^2 \psi}{\partial x^2} + 2S^2 \frac{\partial^2 \psi}{\partial x \partial z} - F^2 \frac{\partial^2 \psi}{\partial z^2} - \mu S^2 \frac{\partial \psi}{\partial x} + \mu F^2 \frac{\partial \psi}{\partial z}$$

$$= -2rf \left(\frac{\partial u_g}{\partial x} \frac{\partial v_g}{\partial z} - \frac{\partial u_g}{\partial z} \frac{\partial v_g}{\partial x} \right). \qquad (2)$$

In (2), f is the Coriolis parameter, which is assumed constant, u_g and v_g are the components of the geostrophic wind velocity in the x (cross-section parallel) and y (cross-section normal) directions, respectively, $N^2 = (g/\theta_0)(\partial\theta/\partial z)$ is a measure of the static stability, $S^2 = f(\partial v_g/\partial z) = (g/\theta_0)(\partial\theta/\partial x)$ is a measure of the baroclinicity and $F^2 = f(f + \partial v_g/\partial x)$ is a measure of the inertial stability. The quantity

$$r = \rho_0 \left(1 - \frac{z}{z_a} \right)^{c_v/R}, \qquad (3)$$

is referred to as the pseudo-density, ρ_0 is a reference density and c_v is the specific heat of dry air at constant volume. The quantity

$$\mu = \frac{c_v}{R} (z - z_a)^{-1} \qquad (4)$$

is the logarithmic derivative of r with respect to z. This term results from accounting for the effects of compressibility in the derivation of (2), which contributes a relatively minor correction to the ψ pattern in the troposphere and lower stratosphere. The stream function ψ is defined so that

$$ru_{ag} = \frac{\partial \psi}{\partial z}, \quad rw = -\frac{\partial \psi}{\partial x}, \qquad (5)$$

where the subscript ag denotes ageostrophic and the vertical velocity w is defined as dz/dt.

The Sawyer–Eliassen equation (2) can be solved provided that lateral boundary conditions are specified and if the ellipticity condition

$$F^2 N^2 - S^4 > 0, \qquad (6)$$

corresponding physically to positive potential vorticity, is satisfied throughout the domain. In the upcoming diagnosis, ψ is assumed to be zero at the lateral and vertical boundaries, and (2) is solved numerically using successive overrelaxation. A recent discussion of the physical interpretation and an example of the application of the Sawyer–Eliassen equation to an upper-level frontal zone appear in Shapiro (1981).

The derivation of (2) requires several restrictive assumptions, which may not be satisfied in the case to be examined. In particular, the ageostrophic circulation is assumed to be two-dimensional and confined to the plane of the cross section. Consequently, contributions to the vertical motion pattern due to stretching or contraction in the direction normal to the cross section, $\partial v_{ag}/\partial y$, are neglected. The ageostrophic circulation can be assumed to be two-dimen-

sional only in special cases involving sufficiently straight frontal zones in which accelerations associated with parcel trajectory curvature are negligible; i.e., the conditions for cross-front geostrophic balance (dv/dt is replaced by dv_g/dt) are satisfied. Next, imposing the condition $\psi = 0$ at the boundaries not only requires the ageostrophic velocity components normal to the boundaries to vanish, but also constrains the vertical domain averages of ru_{ag} and the horizontal domain averages of w to equal zero according to (5). A final restriction is that of constant Coriolis parameter, which is not expected to have a significant effect on the realism of the diagnosed ageostrophic circulations. Several of the above issues will be discussed further later in this section.

The vertical cross section over which ψ is to be diagnosed (see dashed line, Fig. 5b2) extends 2123 km in the x direction with x increasing towards the southwest. The vertical domain extends from $z = 1.73$ km (800 mb)[3] to $z = 11.71$ km (200 mb). The diagnostic grid is unstaggered with uniform spacing and consists of 21 points in the x direction and 14 points in the vertical. Parameters for the diagnosis of ψ include $f = 0.976 \times 10^{-4}$ s^{-1} corresponding to a latitude of 42°N, $\theta_0 = 273$ K, $\rho_0 = 1.276$ kg m^{-3} and $z_a = 27.99$ km. The diagnosis further requires fields of θ, u_g and v_g in order to evaluate the coefficients and forcing of (2). These fields are interpolated to the vertical cross section from objective analyses produced on isentropic surfaces using the scheme described by Petersen (1979). For this particular application, the objective analyses are performed on a horizontal domain with 1° latitude–longitude spacing for 30 uniformly spaced isentropic levels ($\Delta\theta = 4$ K) ranging from 264 to 380 K. Diagnostic quantities, such as the geostrophic wind, are calculated on isentropic surfaces before being interpolated to the vertical cross section.

The analyses of θ, v_g and u_g for 12Z/18 are shown in Fig. 12. The prominent features in the θ and v_g fields are the midtropospheric frontal zone, in which the cross-frontal component of the θ gradient is strongest at about 500 mb, and the associated jet

---

[3] The choice of 800 mb for the lower boundary avoids the necessity of considering the effects of topography, which would complicate the solution of (2). In particular, the lower boundary would no longer correspond to a surface of constant z and thus would be awkward to treat computationally. In view of the dominance of the forcing term in (2) at upper levels (Fig. 13c1), it is felt that this expedient treatment of the lower boundary is justifiable. Nevertheless, the placement of the lower boundary near 800 mb limits the applicability of the derived results. This limitation is associated with the general problem of selecting boundary conditions needed to solve the circulation equation as discussed later in this section. Although the alternative of expressing the circulation equation in terms of terrain-following sigma coordinates is a possibility, it would substantially complicate the form and interpretation of (2).
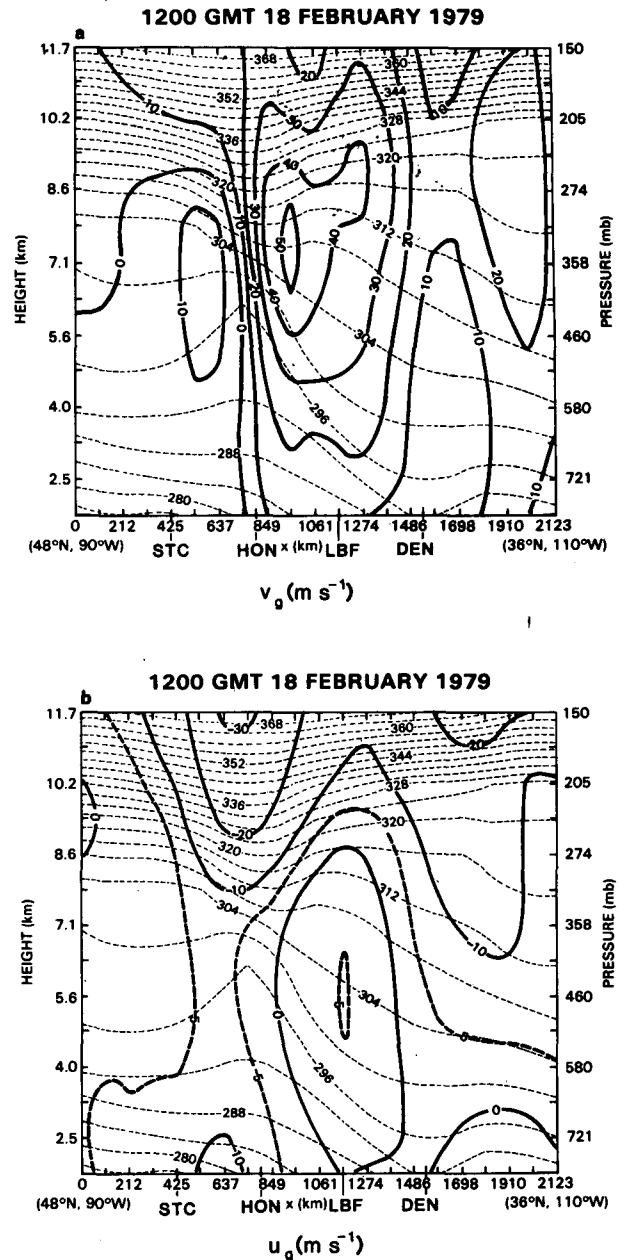

FIG. 12. Vertical cross sections at 1200 GMT 18 February 1979 of potential temperature (contour interval 4 K, thin dashed) and (a) cross-section-normal geostrophic wind component v_g, and (b) cross-section-parallel geostrophic wind component u_g. Geostrophic wind components are denoted by solid lines (contour interval 10 m s^{-1}) and thick dashed lines, which are selected intermediate contours.

streak near the 300 mb level, which is bounded on its poleward flank by a well-defined zone of cyclonic shear in which the absolute vorticity, $f + \partial v_g/\partial x$, reaches $3.8f$. The u_g field contains a 5 m s^{-1} midtropospheric maximum near 1100 km separating diffluence to its left and confluence to its right. Above this maximum, u_g becomes increasingly negative with

FORCING

STREAM FUNCTION

1200 GMT 18 FEBRUARY 1979

1200 GMT 18 FEBRUARY 1979

CONFLUENCE

1200 GMT 18 FEBRUARY 1979

1200 GMT 18 FEBRUARY 1979

HORIZONTAL SHEAR

1200 GMT 18 FEBRUARY 1979

1200 GMT 18 FEBRUARY 1979

TOTAL

FIG. 13. Vertical cross sections at 1200 GMT 18 February 1979 of potential temperature (contour interval 4 K, thin dashed) and 1) forcing to Sawyer–Eliassen circulation equation (contour interval 40×10^{-12} kg m^{-3} s^{-3}, solid) and 2) ageostrophic stream function (contour interval 20×10^2 kg m^{-1} s^{-1}, solid). In (a1)–(c1), thick dashed lines are selected intermediate contours. (a) Confluent forcing and stream function. (b) Horizontal shear forcing and stream function. (c) Total forcing and stream function.

height, indicating that colder air is located upstream (with respect to the jet streak) of the plane of the cross section in the upper troposphere and lower stratosphere. This thermal pattern is evident from the orientation of the isobars relative to the streamline pattern on the 312 K isentropic surface (Fig. 5b2).

Figure 13 displays cross sections of the geostrophic forcing and the associated ψ field partitioned into components due to confluence and horizontal shear, which respectively correspond to the first and second terms on the right of (2). [Note that (2) is formulated so that positive and negative forcing correspond to relative maxima and minima in ψ.] The ψ pattern due to confluence (Fig. 13a2) is dominated in the troposphere by direct and indirect cells respectively forced by confluence and diffluence associated with the midtropospheric u_g maximum. Although the forcing is stronger in the stratosphere than in the troposphere (Fig. 13a1), the response (i.e., the ψ pattern in Fig. 13a2) is weaker in the stratosphere because of the higher static stability. Within the troposphere, the response to the confluent forcing is also amplified and the response to the diffluent forcing is damped on account of respective anticyclonic (small F^2) and cyclonic (large F^2) lateral shears of v_g. The ψ pattern due to horizontal shear forcing (Fig. 13b2) consists of an indirect cell centered in the zone of strong cyclonic shear at the level of maximum v_g and a weaker direct cell situated to the right of the jet, which are forced respectively by cyclonic and anticyclonic shear in the presence of cold advection (Fig. 13b1). When these components are added, the total stream function (Fig. 13c2) is dominated by the indirect cell driven by horizontal shear and the direct cell driven by confluence, which produces a pattern with maximum subsidence on the warm side of the upper-tropospheric frontal zone. The ψ pattern exhibited in Fig. 13c2 resembles that derived by Shapiro (1981, Fig. 12f) in an application of the Sawyer–Eliassen equation to an upper-level frontal system and that shown in the schematic presented by Danielsen (1968, Fig. 14) describing the mean vertical circulation associated with tropopause folding.

As a qualitative verification of the ψ pattern derived from the Sawyer–Eliassen equation, the u_{ag} and w fields computed from (2) and (5) (Fig. 14a) are compared with objectively analyzed two-dimensional circulations (Fig. 14b). The objectively analyzed u_{ag} field is determined from the difference between the u and u_g fields on isentropic surfaces, while the w pattern is determined kinematically by vertically integrating the continuity equation expressed in pressure coordinates following O'Brien (1970). The objectively analyzed ageostrophic circulation contains a zone of strong subsidence maximized within and to the warm side of the upper-tropospheric frontal zone, which agrees favorably with the derived pattern although the analyzed minimum w (-13.4 cm s^{-1}) is signifi-

cantly stronger than the derived minimum w (-6.9 cm s^{-1}). Away from the frontal zone, particularly beyond 1500 km, the agreement between the derived and analyzed circulations is poor in that w is of opposite sign, especially in the southern portion of the cross section.

The lack of detailed agreement between the derived and objectively analyzed ageostrophic circulation patterns in Fig. 14 can be attributed to several factors. First, the objectively analyzed ageostrophic circulation can only be considered an approximate estimate of the true ageostrophic circulation on account of recognized difficulties in inferring ageostrophic motions from radiosonde data, especially in the upper troposphere and lower stratosphere (Shapiro and Kennedy, 1981). Similarly, the derived ageostrophic circulation is at best an inexact estimate of the actual ageostrophic circulation because the assumptions leading to the Sawyer–Eliassen equation are not satisfied completely. The stronger subsidence in the objectively analyzed ageostrophic circulation conforms with expectations of upper-tropospheric along-flow contraction ($\partial v_{ag}/\partial y < 0$) between a ridge and trough that is due to along flow changes in curvature (Shapiro and Kennedy, 1981, Fig. 1; Newton and Trevisan, 1984a). The presence of along-flow variations in v_{ag} is suggested by an objective analysis of the ageostrophic flow on the 312 K isentropic surface (not shown), which indicates downstream (upstream) components of the ageostrophic wind at the ridge (trough) behind (ahead of) the PJ. Consequently, the presence of along-flow contraction violates the assumption of the two-dimensionality of the ageostrophic circulation required for applying (2). Furthermore, the three-dimensionality of the actual flow pattern may also introduce a nondivergent part to the objectively analyzed ageostrophic circulation in contrast to the derived circulation, which is completely irrotational. Nevertheless, if the geostrophic momentum approximation were satisfied, along-flow effects could be accounted for by applying the coupled system of diagnostic ageostrophic circulation equations introduced by Hoskins and Draghici (1977), which are a generalization of the Sawyer–Eliassen equation to three dimensions. Finally, the discrepancies between the objectively analyzed and derived ageostrophic circulations can be attributed to the choice of boundary conditions for the derived case. The presence of rising motion beyond 1500 km in the derived pattern may be a consequence of the constraint that the horizontal domain average of the vertical motion equal zero, which requires compensating ascent adjacent to the descent in the vicinity of the upper-level front.

In summary, there are numerous complications to consider when comparing objectively analyzed circulations with those derived from the two-dimensional Sawyer–Eliassen equation. Nevertheless, despite the discrepancies between the objectively analyzed and

1200 GMT 18 FEBRUARY 1979

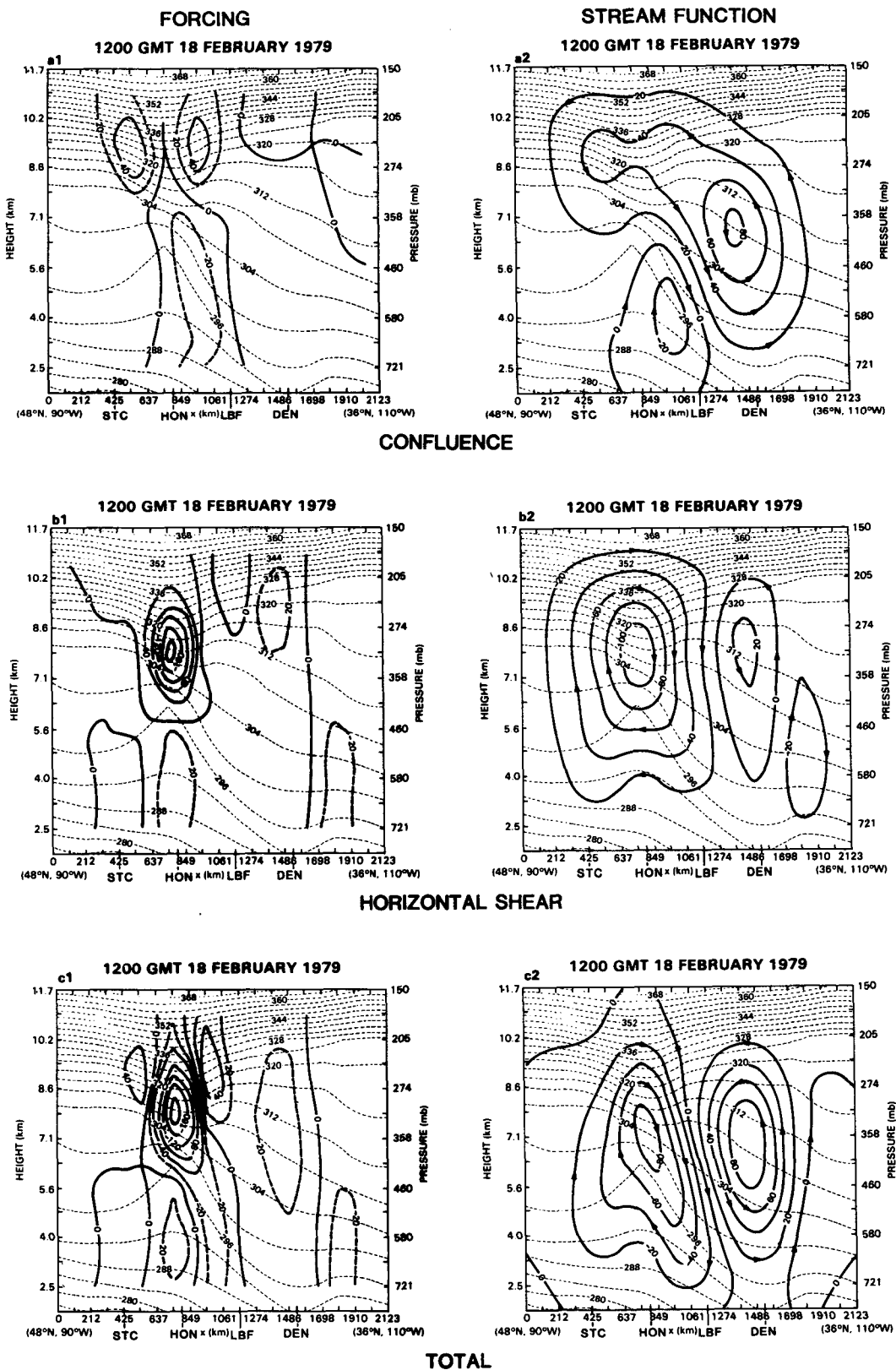SAWYER–ELIASSEN EQUATION

1200 GMT 18 FEBRUARY 1979
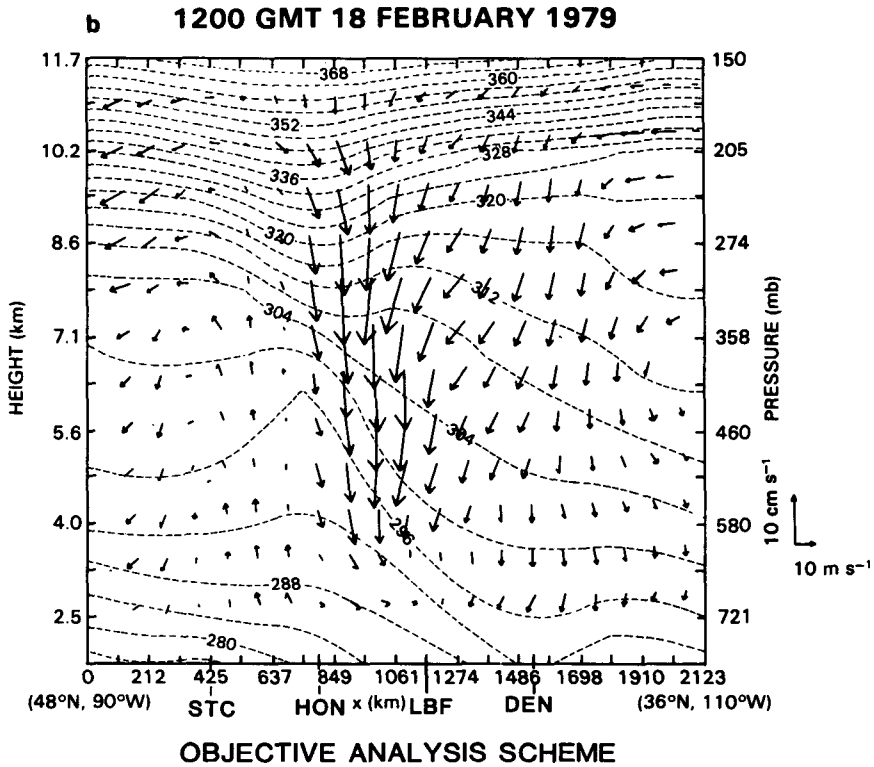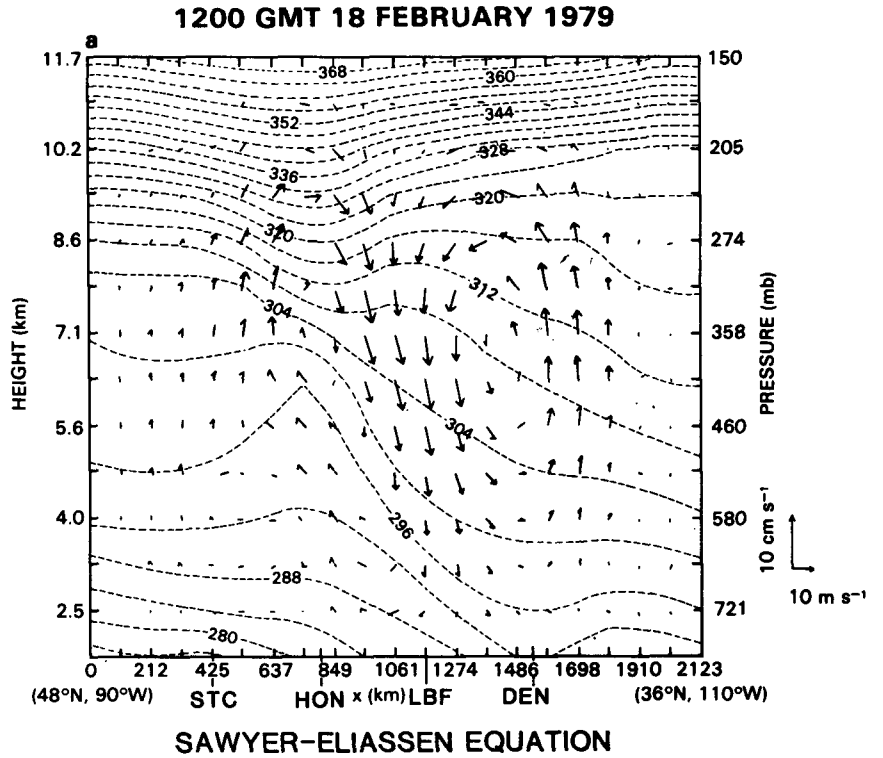

OBJECTIVE ANALYSIS SCHEME

FIG. 14. Vertical cross sections at 1200 GMT 18 February 1979 of potential temperature (contour interval 4 K, dashed) and vector representation of the ageostrophic circulation in the plane of the cross section determined from (a) the Sawyer–Eliassen circulation equation (ψ from Fig. 13c2) and (b) the objective analysis scheme (see text for details).

derived ageostrophic circulation patterns, the subsidence associated with the upper-tropospheric PJ and frontal system is a dominant signal in both approaches for this case. The favorable comparison strongly suggests that synoptic-scale deformation patterns lead to tropopause folding and upper-level frontogenesis by 12Z/18, concentrating the sinking motion along the axis of the PJ between the trough and upstream ridge axes and transporting stratospheric air toward the middle and lower troposphere.

5. Analyses of potential vorticity, static stability and absolute vorticity for the stratospheric air mass

After a review of past attempts to relate tropopause folding to cyclogenesis, analyses of the potential vorticity, static stability and absolute vorticity are presented from Eulerian and Lagrangian perspectives to assess the possible relationship between the extrusion of stratospheric air into the middle and lower troposphere and the rapid cyclogenesis for this case.

a. Background on the relationship between tropopause folding and cyclogenesis

The concept of a tropopause fold complemented the studies of Reed and Sanders (1953) and Newton (1954), which pointed to a growing appreciation of the importance of subsidence in the upper and middle troposphere as a mechanism contributing to upper-level frontogenesis. Reed and Danielsen (1959), Staley (1960), Danielsen (1968, 1980), Reiter (1969), Bosart (1970), Shapiro (1976, 1978, 1980) and Danielsen and Mohnen (1977) discussed the role of tropopause folding in the exchange of air between the stratosphere and troposphere, where the downward extrusion of stratospheric air into the troposphere is marked by high values of potential vorticity, ozone, radioactive material and other chemical constituents.

Several attempts have been made to link the extruded stratospheric air mass to cyclogenesis through the principle of conservation of potential vorticity. As stratospheric air descends into the troposphere, vortex tubes are stretched and static stability decreases significantly. Consequently, absolute vorticity measured on isentropic surfaces is generated following parcel trajectories as long as stratospheric values of potential vorticity are preserved. Kleinschmidt (1950, 1955) was apparently the first to emphasize that the advection of a stratospheric reservoir of high potential vorticity associated with a low tropopause level is an important element in the development of cyclones. The importance of the advection of stratospheric values of potential vorticity into the cyclogenetic region is further stressed by Eliassen and Kleinschmidt (1957) and more recently by Bleck and Mattocks (1984) for numerous ALPEX cyclone cases. Eliassen and Kleinschmidt (1957) go so far as to state that the

stratospheric reservoir marked by high values of potential vorticity "is essentially the producing mass of the cyclones" (p. 125). Both of these studies note that the stratospheric air mass marked by high values of potential vorticity becomes detached from the main stratospheric "reservoir" and subsequently displaced equatorward through some unidentified mechanism. Eliassen and Kleinschmidt hypothesize that a disturbance associated with the jet stream is likely responsible for the detached maximum of potential vorticity in the lower stratosphere and upper troposphere during the period of surface cyclogenesis. Tropopause "folding," as defined by Reed (1955), can be considered to be a mechanism for detaching and transporting stratospheric air from the main "reservoir" toward the middle troposphere along the axis of jet streams.

The work of Staley (1960), Danielsen (1966), Bleck (1973, 1974) and, more recently, Boyle and Bosart (1983) provides supporting evidence for the important role that the downward extrusion of stratospheric air associated with tropopause folding can play in the development of surface cyclones. Staley discusses cyclogenesis in terms of a simultaneous strengthening of the vortex and tropopause folding. Bleck's analysis of numerical simulations of several cyclones and Boyle and Bosart's case study of an East Coast cyclone also emphasize the simultaneous extrusion of stratospheric air into the middle and lower troposphere and surface cyclogenesis.

While the dominant theme of past work has been to relate the simultaneous development of the tropopause fold and cyclogenesis, other studies have indicated that a probable link exists between upper-level frontogenesis and tropopause folding associated with jet streaks and the subsequent development of surface cyclones. Riehl and Teweles (1953) appear to be describing upper-level frontogenesis in their discussion of a developing upper-tropospheric "cold dome," which occurs upstream of the cyclogenetic region and precedes the cyclogenesis by 24 h. Furthermore, they emphasize that their analyses "suggest" that the "downstream propagation of the leading edge of the western jet stream is a link connecting the cold dome in the west and the cyclone formation . . ." (p. 73). Matsumoto et al. (1982) use similar terminology in describing the frontal characteristics during the descent of a "cold dome" within a cold vortex between Korea and Japan which preceded a rapid intensification of an area of precipitation along the east coast of Japan. Their analyses and numerical simulations show a subsiding tropopause and strengthening upper-level front prior to the development of convection and modest amplification of a preexisting surface low. They stress that the deepening low pressure system and associated convection are likely related to the convective instability associated with the advection of cold air over a warm oceanic

planetary boundary layer, while not assessing the possible influence of the vertical frontogenetic circulation associated with the descending cold dome.

Dynamical processes that link jet systems with developing surface cyclones have been emphasized by others such as Petterssen (1956), Newton (1956), Danielsen (1966) and Palmén and Newton (1969). Newton (1956) documents the vortex tube stretching beneath the axis of a jet as it propagates to the lee of the Rocky Mountains and the associated increase in absolute vorticity that marks the developing cyclone. Only Danielsen (1966) specifically discusses the development of the tropopause fold associated with a strong upper-level jet in terms of preceding and subsequently influencing cyclogenesis. However, a detailed diagnostic analysis is not presented by Danielsen to confirm this point.

The diagnostic analyses for the Presidents' Day cyclone which follow are designed to determine if applying the conventional approach (that assumes potential vorticity is conserved, so that absolute vorticity is generated as static stability decreases through adiabatic mass convergence) is adequate for describing the amplification of the mid- to lower-level trough by 12Z/19 and the *subsequent* rapid development of the Presidents' Day cyclone.

b. Eulerian perspective

Potential vorticity, static stability ($\sigma = -\partial\theta/\partial p$; always assumed positive), pressure and absolute vorticity ($\zeta_\theta + f$) on the 292 K surface are illustrated in Fig. 15 for 12Z/18, 00Z/19 and 12Z/19. At 12Z/18, two potential vorticity maxima existed on the 292 K surface (Fig. 15a1). The maximum near the 800 mb level over Kentucky and Tennessee was located downstream of an intense low-level jet within a developing trough (see Fig. 4c1 in Uccellini et al., 1984). By 00Z/19 (Fig. 15a2), either this maximum propagated southeastward to the East Coast or a separate maximum developed near the position of the coastal front and heavy precipitation (as discussed by Bosart and Lin, 1984). The second potential vorticity maximum was located in the central United States at 12Z/18 (Fig. 15a1) on the cyclonic side of the PJ and was associated with the folding event. This potential vorticity maximum was located near the 600 mb level where σ was diagnosed to be less than 5×10^{-2} K mb^{-1} (Fig. 15b1) and $\zeta_\theta + f$ generally above 1.5×10^{-4} s^{-1} (Fig. 15c1), due mostly to the strong cyclonic shear associated with the PJ.

By 00Z/19, the potential vorticity maximum moving with the PJ was located in southern Illinois (Fig. 15a2) nearly 500 km downstream of the ozone maximum measured by TOMS on 18 February (Fig. 11b). Trajectories computed by Petersen and Homan (1984) indicate that parcels initialized along the axis of the PJ at 12Z/18 passed through southern Iowa

near 1800 GMT and terminated in the potential vorticity maximum over Illinois at 00Z/19, confirming that the potential vorticity and ozone maxima (Fig. 11b) describe the same feature. The potential vorticity maximum had descended to a pressure level between 600 and 700 mb, had doubled in magnitude, and was located at the base of the intensifying trough, where σ had increased to values larger than 7×10^{-2} K mb^{-1} (Fig. 15b2) with $\zeta_\theta + f$ remaining above 1.5×10^{-4} s^{-1} (Fig. 15c2). The descent of the maximum potential vorticity to higher pressure beneath the axis of the PJ occurred within the northernmost dry band in the THIR 6.7 μm image (Fig. 4a) and is consistent with the hypothesis that stratospheric air was transported into the lower troposphere by the sinking motion diagnosed within the baroclinic zone associated with the PJ (Figs. 6a, 7a, and 14). The magnitude of the potential vorticity increased by a factor of 2 between 12Z/18 and 00Z/19. Similar increases in potential vorticity during stratospheric extrusions have been noted by Eliassen and Kleinschmidt (1957), Bleck and Mattocks (1984) and Bosart and Lin (1984). These increases are due either to deficiencies in the data base and analysis scheme or to nonconservative, diabatic processes (Staley, 1960; Shapiro, 1976, 1978; Gidel and Shapiro, 1979). (See the Appendix for further discussion of the possible influence of diabatic processes in increasing the potential vorticity for this case.)

By 12Z/19, the potential vorticity maximum associated with the PJ–trough system was located over Virginia (Fig. 15a3). The magnitude of the potential vorticity centered over Virginia at 12Z/19 now *decreased*, which could again be related to diabatic processes (as noted by Staley, 1960) or to data limitations arising from a nonuniform distribution of radiosondes and a critical data gap at 12Z/19 when the sounding at Dulles International Airport (IAD) was missing. Nevertheless, the analyses show that the air mass with potential vorticity greater than 10×10^{-6} K mb^{-1} s^{-1} had descended still further to the 600–800 mb layer as it moved toward the Mid-Atlantic Coast (Fig. 15b3). The potential vorticity maxima at 12Z/18, 00Z/19 and 12Z/19, and the TOMS ozone measurements on 18 and 19 February (Fig. 11), yield a distinct path from the position of the tropopause fold over the central United States on 18 February to the site of rapid cyclogenesis off the East Coast on the following day. However, as is shown in the trajectory analysis which follows, a complicating factor in tracking the stratospheric air mass toward the East Coast is that the northern portion of the potential vorticity maximum in Virginia at 12Z/19 was also affected by the advection of air from the potential vorticity maximum located in the Carolinas at 00Z/19 (Fig. 15a2).

As the potential vorticity maximum propagated toward the East Coast, the static stability (σ) down-
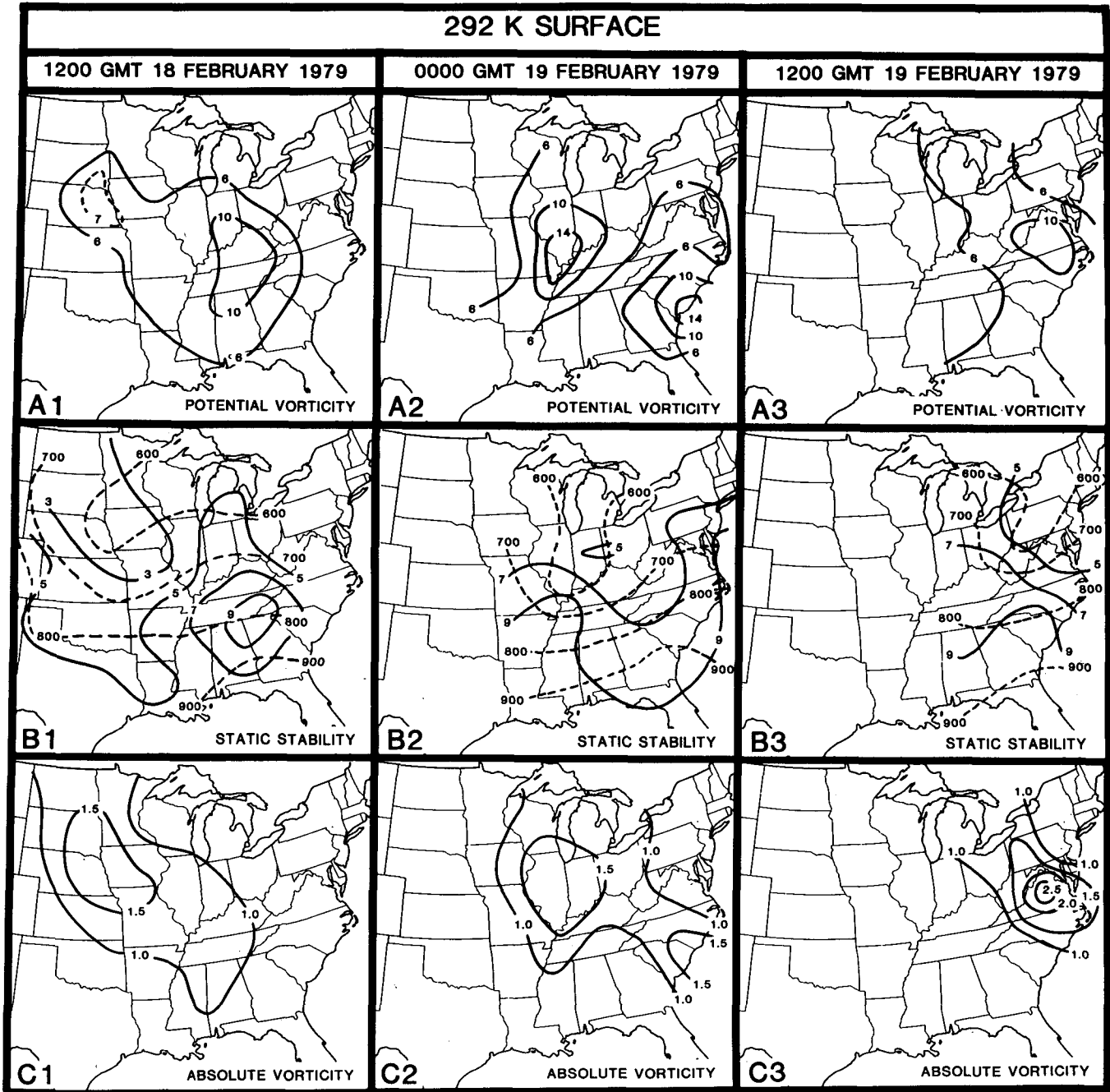
292 K SURFACE

| 1200 GMT 18 FEBRUARY 1979 | 0000 GMT 19 FEBRUARY 1979 | 1200 GMT 19 FEBRUARY 1979 |

FIG. 15. Isentropic analyses for 292 K surface of (a) potential vorticity $(10 = 10 \times 10^{-6}$ K mb^{-1} s$^{-1})$; (b) static stability (solid, $5 = 5 \times 10^{-2}$ K mb^{-1}) and pressure (dashed, mb); (c) absolute vorticity $(1.5 = 1.5 \times 10^{-4}$ s$^{-1})$. The left 1), center 2), and right 3) columns are for 1200 GMT 18 February, 0000 GMT 19 February, and 1200 GMT 19 February 1979, respectively.

stream of the trough axis decreased from 7×10^{-2} K mb^{-1} in southern Illinois and Kentucky at 00Z/19 (Fig. 15b2) to 5×10^{-2} K mb^{-1} over Virginia (Fig. 15b3). The local change of σ in isentropic coordinates is related to the adiabatic and diabatic mass convergence through the expression

$$\partial\sigma/\partial t = \sigma^2\left[\nabla_\theta\cdot(\sigma^{-1}\mathbf{U}) + \frac{\partial}{\partial\theta}(\sigma^{-1}\dot\theta)\right], \quad (7)$$

where σ increases (decreases) with mass divergence (convergence). The decrease of σ as the PJ–trough system moved toward Virginia between 00Z/19 and 12Z/19 was associated with the increasing areal-averaged lower-tropospheric mass convergence diagnosed downstream of the trough axis (Figs. 7b and 8b). By 12Z/19, a -50×10^{-6} mb K^{-1} s^{-1} maximum in the adiabatic mass convergence (Fig. 16) was located immediately downwind of the trough axis,
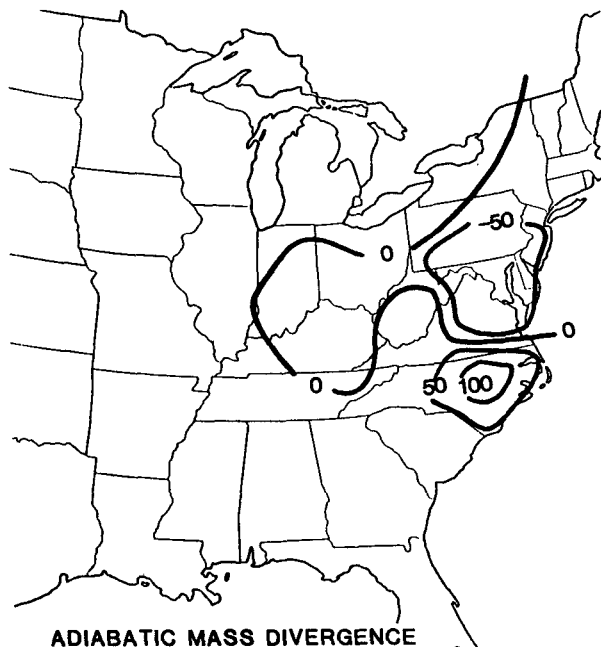
FIG. 16. Adiabatic mass divergence for the 292 K surface at 1200 GMT 19 February 1979 (50 = 50 × 10⁻⁶ mb K⁻¹ s⁻¹).

extending from southern Virginia northward to central Pennsylvania, where the static stability decreased between 00Z/19 and 12Z/19 (Figs. 15b2 and 15b3).

Coinciding with the decrease in σ along the 292 K surface between 00Z/19 and 12Z/19, the maximum of $\zeta_\theta + f$ on the 292 K surface increased significantly from 1.7×10^{-4} s⁻¹ over Illinois at 00Z/19 (Fig. 15c2) to greater than 2.5×10^{-4} s⁻¹ over Virginia by 12Z/19 (Fig. 15c3). The increase in the maximum $\zeta_\theta + f$ on the 292 K surface occurred as the lower-tropospheric mass convergence near and downstream of the trough axis (Figs. 7b and 8b) acted to decrease the static stability and to stretch vortex tubes immediately upstream of the developing cyclone. Therefore, it appears that the potential for an increase in the absolute vorticity marking the stratospheric air mass located over the midwestern United States at 00Z/19 was being realized between the 600 and 800 mb levels by 12Z/19 as the air mass was advected toward the East Coast.

c. Lagrangian perspective

In order to attempt to use the conservation of potential vorticity to relate the increase in the absolute vorticity on isentropic surfaces to the decrease in static stability over Virginia, trajectories were computed on the 292 K surface during the 12 h between 00Z/19 and 12Z/19 using a discrete model approach (Petersen and Uccellini, 1979). Uccelini et al. (1984) discuss recent modifications and limitations of the trajectory method when used with the operational

radiosonde network in which data are available only at 12 h intervals. Nevertheless, the explicit trajectory scheme combined with the Petersen objective analysis scheme yielded approximately 30 trajectories initialized in the central and southeastern United States that could be used to diagnose changes in potential vorticity, σ and $\zeta_\theta + f$ between 00Z/19 and 12Z/19.

Figure 17 shows three representative trajectories that were initialized near the 600 mb level within the potential vorticity maximum on the 292 K surface and which spread out in a manner similar to the schematic presented by Danielsen (1980, Fig. 12). The 00Z/19 and 12Z/19 values of pressure, potential vorticity, static stability and absolute vorticity are listed in Table 1 for the three parcels. Parcels 1 and 2 are representative of those that were initialized respectively to the west of and on the trough axis at 292 K. During the first 3 h, many of these parcels had speeds which were less than the propagation rate of the trough. Thus, the parcels remained to the west and southwest of the trough axis. As indicated by trajectories 1 and 2, these parcels decelerated and turned toward the right, descending to pressure levels greater than 800 mb. At 12Z/19, parcels 1 and 2 were located near the axis of the maximum potential vorticity that extended from Virginia southwestward toward the Gulf of Mexico (Fig. 15a3). However, as Table 1 indicates for parcels 1 and 2, the potential
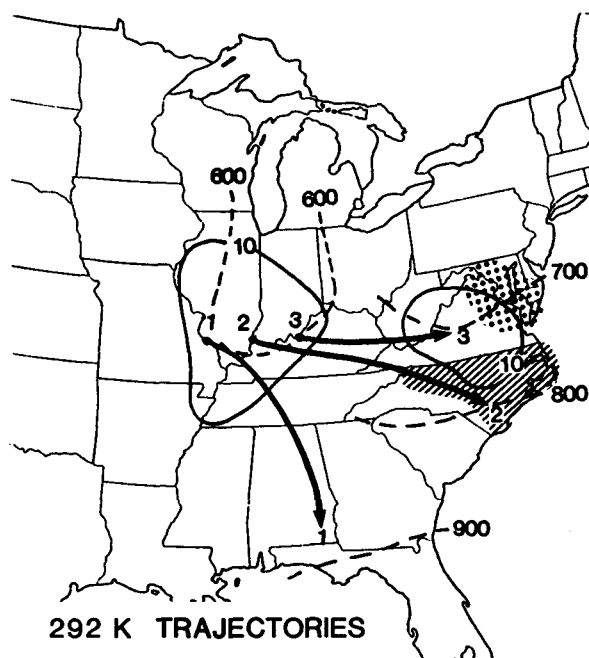
292 K TRAJECTORIES

FIG. 17. Display of three trajectories on 292 K surface for period between 0000 GMT and 1200 GMT 19 February 1979 with initial and end points numbered. Pressure (dashed lines) and potential vorticity (light solid) analyses from Fig. 15 included for the initial and final times. Stippled region (centered near Virginia–Maryland border at 12 Z/19) contains end points of trajectories that were initialized in hatched region (North Carolina) at 00 Z/19.

vorticity was not conserved for the parcels that descended below 800 mb, nor was the expected relationship between changes in σ and $\zeta_\theta + f$ confirmed. The lack of conservation in the potential vorticity is related perhaps to analysis deficiencies, as noted earlier, or to diabatic and frictional processes as these trajectories approached the planetary boundary layer.

Parcel 3 is representative of the parcels initialized in the eastern portion of the potential vorticity maximum, located east of the trough axis near the 600 mb level. These trajectories remained near the trough

TABLE 1. Values of pressure, potential vorticity, static stability, and absolute vorticity measured on isentropic surfaces at the initial and final points of parcel trajectories on the 292 K surface between 00 Z/19 and 12 Z/19 (Fig. 17). Values at 00 Z/19 are listed to left, while values at 12 Z/19 are in parentheses to the right in each column.

Parcel	Pressure (mb)	Potential vorticity $(10^{-6} \text{ K mb}^{-1} \text{ s}^{-1})$	Static stability $(10^{-2} \text{ K mb}^{-1})$	Absolute vorticity (10^{-4} s^{-1})
1	610 (880)	14.0 (5.0)	8.0 (10.)	1.7 (0.5)
2	580 (800)	17.0 (9.2)	8.3 (7.1)	2.1 (1.3)
3	600 (700)	11.0 (11.)	6.7 (5.1)	1.7 (2.2)

axis on the 292 K surface and terminated near the 700 mb level, above the planetary boundary layer and within the potential vorticity maximum analyzed over Virginia at 12Z/19. Table 1 shows that the potential vorticity for parcel 3 was conserved, with σ decreasing from 6.7 to 5.1 $\times$ 10^{-2} K mb^{-1} and ζ_θ + f increasing from 1.7 to 2.2 $\times$ 10^{-4} s^{-1}. This trajectory computation provides supporting evidence that the descent of the stratospheric air mass to the 700–800 mb layer in the Middle Atlantic states (Figs. 15a3 and 15b3) and the decrease in σ related to the adiabatic mass convergence (Figs. 7b, 8b, and 16) accompanied the increase in absolute vorticity immediately upwind of the region of rapid cyclogenesis.

In Fig. 17, the stippled region near the northeastern portion of the potential vorticity maximum at 12Z/19 represents the area in which trajectories terminated for parcels originating in North Carolina at 00Z/19 (hatched region) within the northern edge of the potential vorticity maximum analyzed along the Southeast Coast (Fig. 15a2). As was the case for parcel 3, these parcels (not shown) nearly conserved their potential vorticity values (approximately 8.0 $\times$ 10^{-6} K mb^{-1} s^{-1}), experienced a significant decrease in σ and an associated increase in $\zeta_\theta + f$. Unlike the parcels originating within the stratospheric extrusion that were descending toward the East Coast, these parcels *ascended* the isentropic surface, rising from 800 mb at 00Z/19 to a pressure level less than 700 mb by 12Z/19. These trajectory results indicate that the potential vorticity maximum in Virginia at 12Z/19 was not only comprised of stratospheric air originating in the folded tropopause, but also of air originating in the lower troposphere to the south of

the developing cyclone. This result is consistent with the concept that the interaction between the PJ-trough and the preexisting coastal front was an important factor in the overall evolution of the storm system, as discussed by Uccellini et al. (1984) and Bosart and Lin (1984). However, given the lack of data off the East Coast, it is beyond the scope of this paper to assess the exact means by which this interaction evolved and contributed to an increase in absolute vorticity associated with the development of the cyclone.

d. Discussion

The nonconservative aspects of the potential vorticity analysis introduce a level of uncertainty as to its exact evolution during the precyclogenetic period. Nevertheless, the Eulerian and Lagrangian results combined with the TOMS and THIR data indicate that the potential for a significant increase in the absolute vorticity, which marks the stratospheric air extruded downward within the tropopause fold, was being realized below the 600 mb level upstream of the East Coast between 00Z/19 and 12Z/19 prior to the explosive development of the Presidents' Day cyclone. The increase in absolute vorticity in the lower to middle troposphere was related, in part, to vertical stretching of the stratospheric air as it descended toward the lower troposphere and then approached the East Coast. Another factor in this case was the interaction of the descending stratospheric air with the ascending air within the western portion of the inverted trough, which not only added another source of high potential vorticity but also contributed to the decrease in σ and associated increase in $\zeta_\theta + f$ below 600 mb between 00Z/19 and 12Z/19.

An analysis of the potential vorticity, σ and $\zeta_\theta + f$ for the explosive development phase of the Presidents' Day cyclone is not possible because of the lack of upper-air data over the ocean. However, the TOMS ozone analysis (Fig. 11c) and THIR water vapor imagery (Fig. 4b) indicate that the descending stratospheric air located over Virginia at 12Z/19 (marked by an x in Fig. 11c) was nearly colocated with the developing vortex by 1637 GMT. The TOMS and THIR analyses support an interpretation that stratospheric air was brought down to the oceanic boundary layer, which was being influenced by diabatic processes before and during the cyclogenesis.[4] Potential vorticity

---

[4] See Fig. 22 in Bosart (1981), which shows an average potential temperature exceeding 288 K for the lowest 50 mb immediately off the Middle Atlantic Coast. The application of this estimate to the 12 Z/19 Wallops Island radiosonde report yields a dry adiabatic layer from the surface up to 800 mb, which is consistent with Bosart's contention that warming of the oceanic boundary layer due to sensible heating could have created a 100 to 200 mb deep layer in which lapse rates would have been nearly dry adiabatic.

conservation in the isentropic framework is an inappropriate constraint under these conditions, indicating that processes in addition to vortex tube stretching, and likely influenced by weak static stability in the oceanic boundary layer, could have contributed to the rapid cyclogenesis off the East Coast.

Since diabatic processes appear to be important for the coastal cyclone, it may be preferable to use the pressure-coordinate form of the vorticity equation to describe the rapid development of the vortex. Tilting effects have been shown to be important in the increase of absolute vorticity in the lower troposphere along the East Coast prior to 12Z/19 (Bosart and Lin, 1984). With the large vertical wind shears directed essentially from the west in the lower and middle troposphere, it is possible that the tilting effect associated with differential vertical motions near the storm may have been even more important after 12 Z/19. The descent of the stratospheric air mass (marked by strong westerly winds) toward the planetary boundary layer to the south of the low center and the ascent in the region of strong low-level easterly winds to the north of the low center (where the rising motion was likely enhanced by latent heat release) could have combined to increase the lower-tropospheric cyclonic circulation during the explosive developing stage of the cyclone. Unfortunately, the relative contributions of vertical stretching, tilting effects and nonconservative processes to the increase in cyclonic vorticity could not be diagnosed after 12 Z/19 from the operational radiosonde data base.

6. Summary

An analysis of the Presidents' Day cyclone of 18–19 February 1979, based on conventional radiosonde data, SMS-GOES infrared and visible satellite imagery, water vapor images from the Temperature Humidity Infrared Radiometer (THIR), and ozone measurements from the Total Ozone Mapping Spectrometer (TOMS), is presented to study the relationship between tropopause folding associated with an amplifying polar jet (PJ)–trough system and cyclogenesis. The diagnostic analyses indicate that scale-interactive, dynamically forced vertical circulations played an important role in the extrusion of stratospheric air along the axis of a polar jet and the overall development of the storm system. Synoptic-scale geostrophic deformation led to mesoscale circulation patterns near the PJ which were found to have contributed to a band of strong descent on the warm side of a developing upper-level front along and beneath the axis of the PJ. Vertical stretching of the stratospheric air mass downstream of the folded tropopause and the interaction of the PJ–trough system with the inverted trough–coastal front along the East Coast subsequently contributed to a noticeable increase in the absolute vorticity in the lower troposphere associated with the rapid cyclogenesis along the coast.

Specific findings from the case study include:

1) The amplification of the PJ–trough system occurred in the central United States 12 to 24 h prior to rapid cyclogenesis. The amplifying PJ–trough was first marked by strong subsidence along the axis of the PJ between the trough and upstream ridge axes as early as 12Z/18. It was not until 00Z/19 and 12 Z/19, however, that a coherent two-layer mass divergence pattern, significant upward vertical motion and the resultant rapid expansion of a deep cloud cover and heavy snow developed in the area downstream of the trough axis.

2) A tropopause fold was associated with an intensifying PJ–trough system, and the formation of the fold was related to the subsidence forced by geostrophic deformation patterns connected with the jet streak.

3) The folding process extruded dry stratospheric air (marked by high values of potential vorticity) down toward the 700 mb level 1500 km upstream of the East Coast prior to the explosive development of the cyclone. This result differs from the emphasis of previous case studies, which have examined the concurrent development of a folded tropopause and cyclogenesis, since the appearance of the tropopause fold preceded the rapid development of the cyclone by 12 to 24 h.

4) During the 12 h preceding rapid cyclogenesis, the stratospheric air continued moving toward the East Coast and descended toward the 800 mb level. The Eulerian and Lagrangian diagnostics indicate that, even though the upper-level trough (at the 312 K level) no longer amplified and potential vorticity was not strictly conserved, the absolute vorticity increased in the lower to middle troposphere (at the 292 K level) in association with the increasing mass convergence and subsequent vertical stretching in the region downstream of the trough axis. These changes occurred upstream of the region in which the explosive cyclogenesis commenced.

5) The SMS-GOES infrared and visible satellite imagery, the THIR water vapor imagery and the TOMS ozone measurements, combined with Bosart's (1981) analysis of the oceanic boundary layer, all indicate that the stratospheric air mass was nearly colocated with the region of warmest boundary layer temperatures near the developing vortex as rapid deepening occurred with a noticeable cloud-free eye at the storm center. This result suggests that the explosive development of the cyclone continued to be affected in some undetermined manner by the descent of stratospheric air toward the planetary boundary layer over the Atlantic Ocean. However, the use of potential vorticity as a constraint identifying the potential for an increase in absolute vorticity does not imply that vertical stretching was the only process that contributed to the formation of the Presidents' Day cyclone. The relative contributions of the vertical

stretching of the stratospheric air mass and nonconservative diabatic processes (especially those which act to weaken the static stability in the oceanic planetary boundary layer) to the rapid vortex development off the East Coast could not be diagnosed from the operational radiosonde data base.

Several other important questions could not be resolved with our diagnostic analysis and remain for future research. The analysis of the tropopause fold showed significant increases in potential vorticity on isentropic surfaces in conjunction with increased static stability in the frontal zone. These results are consistent with Eliassen and Kleinschmidt's (1957) analysis of a cyclone over the central United States, which suggests that diabatic processes might have produced potential vorticity in the frontal zone and, in turn, possibly influenced the meso-α scale circulation. More research is needed with better data sets to determine if this upscale influence in fact occurs, as postulated by Shapiro (1976, 1978), since the ramifications for the predictability of a certain class of rapidly developing cyclones and subsequent modifications to the larger-scale flow pattern would be significant. Continued research on upper-level frontogenesis and tropopause folding near jets would also help to define the vertical resolution needed in numerical models to simulate properly the folding process and its subsequent role in rapid cyclogenesis.

Finally, the results from this case study may be applicable to other cases of rapid cyclogenesis. Potential vorticity analyses by Bleck and Mattocks (1984) and aircraft ozone analyses by Buzzi et al. (1984) for the 24–25 April 1982 ALPEX cyclone case indicate that a stratospheric extrusion was observed over central Europe on 24 April in advance of the rapid cyclogenesis in the Gulf of Genova on 25 April 1982. Cross-section analysis and TOMS imagery (not shown) for the 5–6 April 1982 spring blizzard in the northeastern United States indicate that tropopause folding over the Great Lakes region preceded the rapid vortex formation off the New York coast by 12 to 24 h. Similarly, vertical cross sections extending from southeastern Canada to the northeastern United States for 1200 GMT 9 September 1978 (not shown) reveal a distinct tropopause fold along the axis of a strong jet system imbedded within a short wave upstream of the area in which the QE II storm rapidly developed. (See Gyakum, 1983a,b, for a description of the QE II storm.) Again, the relative contribution of the stratospheric extrusion and nonconservative diabatic processes for these and other cases could only have been assessed with more extensive data sets. For the Presidents' Day storm, radiosonde data sets with increased temporal resolution over a region at least 1500 to 2000 km upstream of the developing cyclone and extending over the ocean would have been needed to diagnose fully 1) the changes which occurred during the folding processes in the 12 h between 12

Z/18 and 00Z/19, 2) the apparent interaction between the stratospheric air and the inverted trough-coastal front by 12Z/19, and 3) the rapid vortex formation in the 6–9 h period after 12Z/19. Future studies attempting to address these issues with improved data sets (such as the Genesis of Atlantic Lows Experiment—GALE) or with numerical model simulations will help increase our understanding of the dynamical scale interactions and the relationships between adiabatic and diabatic processes that lead to explosive oceanic cyclogenesis along the coasts of major continents.

APPENDIX

Nonconservative Aspects of Potential Vorticity Analysis

The increased magnitude of the potential vorticity maximum as it moved from eastern Nebraska at 12 Z/18 to southern Illinois at 00Z/19 is related to increased values of static stability shown in the cross section (Fig. 10b) and on the 292 K surface (Fig. 15b2). The absolute vorticity associated with the potential vorticity maximum remained nearly constant. The sensitivity of potential vorticity computations to the analysis of static stability has been stressed by Bleck and Mattocks (1984). Filtering the static stability analysis tends to reduce the magnitude of the potential vorticity at 00Z/19. However, the application of the filter to the 12Z/18 static stability analysis causes a similar decrease in the magnitude of the potential vorticity. Thus, however the data are smoothed, the net effect is still a significant *increase* in the potential vorticity on the 292 K and other isentropic surfaces within the frontal zone. Consequently, this increase in potential vorticity may be a

result of diabatic processes related to a combination of latent heating, turbulent heat fluxes and radiative processes (Staley, 1960; Shapiro, 1976, 1978; Gidel and Shapiro, 1979). Gidel and Shapiro specifically note that clear-air turbulence in regions of strong vertical wind shear in upper-level frontal zones is capable of generating potential vorticity at the level of maximum wind. Perhaps, in this case, turbulence associated with the polar jet and radiative cooling immediately above clouds that were "capped" by the frontal zone combined to produce a heating profile capable of generating a significant increase in the potential vorticity as analyzed in Figs. 15a1 and 15a2. Moisture profiles from individual soundings confirm that the vertical extension of the saturated portion of the sounding was capped by the stable dry air marking the frontal zone. However, the deficiencies in the data base prevent us from drawing any definite conclusions concerning this aspect of the problem.

REFERENCES

Bleck, R., 1973: Numerical forecasting experiments based on the conservation of potential vorticity on isentropic surfaces. *J. Appl. Meteor.*, **12**, 737-752.

——, 1974: Short-range prediction in isentropic coordinates with filtered and unfiltered numerical models. *Mon. Wea. Rev.*, **102**, 813-829.

——, and C. Mattocks, 1984: A preliminary analysis of the role of potential vorticity in Alpine lee cyclogenesis. *Beitr. Phys. Atmos.*, **57**, 357-368.

Bosart, L. F., 1970: Mid-tropospheric frontogenesis. *Quart. J. Roy. Meteor. Soc.*, **96**, 442-471.

——, 1981: The Presidents' Day snowstorm of 18-19 February 1979: A subsynoptic-scale event. *Mon. Wea. Rev.*, **109**, 1542-1566.

——, and S. C. Lin, 1984: A diagnostic analysis of the Presidents' Day storm of February 1979. *Mon. Wea. Rev.*, **112**, 2148-2177.

Boyle, J. S., and L. F. Bosart, 1983: A cyclone/anticyclone couplet over North America: An example of anticyclone evolution. *Mon. Wea. Rev.*, **111**, 1025-1045.

Bhartia, P. K., K. F. Klenk, C. K. Wong and D. Gordon, 1984a: Intercomparison of NIMBUS 7 SBUV/TOMS total ozone data sets with Dobson and M83 results. *J. Geophys. Res.*, **89**, 5239-5247.

——, ——, A. J. Fleig, C. G. Wellemeyer and D. Gordon, 1984b: Intercomparison of NIMBUS 7 solar backscattered ultraviolet ozone profiles with rocket, balloon and umkehr profiles. *J. Geophys. Res.*, **89**, 5227-5238.

Buzzi, A., G. Giovanelli, T. Nanni and M. Tagliazucca, 1984: Study of high ozone concentrations in the troposphere associated with lee cyclogenesis during ALPEX. *Beitr. Phys. Atmos.*, **57**, 380-392.

Danielsen, E. F., 1964: *Project Springfield Report.* Defense Atomic Support Agency, Washington, DC 20301, DASA-1517, 97 pp. [NTIS AD-607980.]

——, 1966: Research in four-dimensional diagnosis of cyclonic storm cloud systems. Rep. No. 66-30, Air Force Cambridge Res. Lab., Bedford, MA, 53 pp. [NTIS AD-632668.]

——, 1968: Stratospheric-tropospheric exchange based upon radioactivity, ozone, and potential vorticity. *J. Atmos. Sci.*, **25**, 502-518.

——, 1980: Stratospheric source for unexpectedly large values of ozone measured over the Pacific Ocean during GAMETAG, August 1977. *J. Geophys. Res.*, **85**, 401-412.

——, and V. A. Mohnen, 1977: Project Dustorm report: Ozone transport, in situ measurements, and meteorological analyses of tropopause folding. *J. Geophys. Res.*, **82**, 5867-5877.

Eliassen, A., 1962: On the vertical circulation in frontal zones. *Geofys. Publ.*, **24**, 147-160.

——, and E. Kleinschmidt, 1957: Dynamic meteorology. *Handbuch der Physik*, Vol. 48, J. Bartels, Ed., Springer-Verlag, 1-154.

Gidel, L. T., and M. A. Shapiro, 1979: The role of clear air turbulence in the production of potential vorticity in the vicinity of upper tropospheric jet stream-frontal systems. *J. Atmos. Sci.*, **36**, 2125-2138.

Gyakum, J. R., 1983a: On the evolution of the *QE II* storm. I: Synoptic aspects. *Mon. Wea. Rev.*, **111**, 1137-1155.

——, 1983b: On the evolution of the *QE II* storm. II: Dynamic and thermodynamic structure. *Mon. Wea. Rev.*, **111**, 1156-1173.

Heckley, W. A., and B. J. Hoskins, 1982: Baroclinic waves and frontogenesis in a non-uniform potential vorticity semi-geostrophic model. *J. Atmos. Sci.*, **39**, 1999-2016.

Hoskins, B. J., and F. P. Bretherton, 1972: Atmospheric frontogenesis models: Mathematical formulation and solution. *J. Atmos. Sci.*, **29**, 11-37.

——, and I. Draghici, 1977: The forcing of ageostrophic motion according to the semigeostrophic equations and in an isentropic coordinate model. *J. Atmos. Sci.*, **34**, 1859-1867.

Kleinschmidt, E., 1950: Über Aufbau und Entstehung von Zyklonen (1. Teil). *Meteor. Rundsch.*, **3**, 1-6.

——, 1955: Die Entstehung einer Höhenzyklone über Nordamerika. *Tellus*, **7**, 96-110.

Krishnamurti, T. N., 1968: A study of a developing wave cyclone. *Mon. Wea. Rev.*, **96**, 208-217.

Matsumoto, S., K. Ninomiya, R. Hasegawa and Y. Miki, 1982: The structure and the role of a subsynoptic-scale cold vortex on the heavy precipitation. *J. Meteor. Soc. Japan*, **60**, 339-353.

Mudrick, S. E., 1974: A numerical study of frontogenesis. *J. Atmos. Sci.*, **31**, 869-892.

Newton, C. W., 1954: Frontogenesis and frontolysis as a three-dimensional process. *J. Meteor.*, **11**, 449-461.

——, 1956: Mechanisms of circulation change during lee cyclogenesis. *J. Meteor.*, **13**, 528-539.

——, and A. Trevisan, 1984a: Clinogenesis and frontogenesis in jet-stream waves. Part I: Analytical relations to wave structure. *J. Atmos. Sci.*, **41**, 2717-2734.

——, and A. Trevisan, 1984b: Clinogenesis and frontogenesis in jet-stream waves. Part II: Channel model numerical experiments. *J. Atmos. Sci.*, **41**, 2735-2755.

O'Brien, J. J., 1970: Alternative solutions to the classical vertical velocity problem. *J. Appl. Meteor.*, **9**, 197-203.

Palmén, E., 1951: The aerology of extratropical disturbances. *Compendium of Meteorology*, T. F. Malone, Ed., Amer. Meteor. Soc., 599-620.

——, and C. W. Newton, 1969: Atmospheric circulation systems: Their structure and physical interpretation. *International Geophysical Series*, Vol. 13, Academic Press, 603 pp.

Petersen, R. A., 1979: A cross-sectional approach to three-dimensional analysis. *Preprints 4th Conf. Numerical Weather Prediction*, Silver Spring, Amer. Meteor. Soc., 35-42.

——, and L. W. Uccellini, 1979: The computation of isentropic atmospheric trajectories using a "discrete model" approach. *Mon. Wea. Rev.*, **107**, 566-574.

——, and J. H. Homan, 1984: A simple Lagrangian forecast system with aviation forecast potential. *Preprints 9th Conf. Aerospace and Aeronautical Meteorology*, Omaha, Amer. Meteor. Soc., 123-128.

——, L. W. Uccellini, A. Mostek and D. A. Keyser, 1984: Delineating mid- and low-level water vapor patterns in a preconvective environment using VAS moisture channels. *Mon. Wea. Rev.*, **112**, 2178-2198.

Petterssen, S., 1956: *Weather Analysis and Forecasting. Vol. 1*, 2nd ed., McGraw-Hill, 428 pp.

Reed, R. J., 1955: A study of a characteristic type of upper-level frontogenesis. *J. Meteor.*, **12**, 226-237.

——, and F. Sanders, 1953: An investigation of the development of a mid-tropospheric frontal zone and its associated vorticity field. *J. Meteor.,* **10,** 338–349.

——, and E. F. Danielsen, 1959: Fronts in the vicinity of the tropopause. *Arch. Meteor. Geophys. Bioklim.,* **A11,** 1–17.

Reiter, E. R., 1969: Tropopause circulation and jet streams. *World Survey of Climatology, Vol. 4: Climate of the Free Atmosphere,* D. F. Rex, Ed, Elsevier, 85–193.

Riehl, H., and S. Teweles, 1953: A further study on the relation between the jet stream and cyclone formation. *Tellus,* **5,** 66–79.

Rodgers, E. B., V. V. Salomonson and H. L. Kyle, 1976: Upper tropospheric dynamics as reflected in Nimbus 4 THIR 6.7-μm data. *J. Geophys. Res.,* **81,** 5749–5758.

Sawyer, J. S., 1956: The vertical circulation at meteorological fronts and its relation to frontogenesis. *Proc. Roy. Soc. London,* **A234,** 346–362.

Schoeberl, M. R., and A. J. Krueger, 1983: Medium scale disturbances in total ozone during southern hemisphere summer. *Bull. Amer. Meteor. Soc.,* **64,** 1358–1364.

Shapiro, M. A., 1970: On the applicability of the geostrophic approximation to upper-level frontal-scale motions. *J. Atmos. Sci.,* **27,** 408–420.

——, 1975: Simulation of upper-level frontogenesis with a 20-level isentropic coordinate primitive equation model. *Mon. Wea. Rev.,* **103,** 591–604.

——, 1976: The role of turbulent heat flux in the generation of potential vorticity in the vicinity of upper-level jet stream systems. *Mon. Wea. Rev.,* **104,** 892–906.

——, 1978: Further evidence of the mesoscale and turbulent structure of upper level jet stream-frontal zone systems. *Mon. Wea. Rev.,* **106,** 1100–1111.

——, 1980: Turbulent mixing within tropopause folds as a mech-anism for the exchange of chemical constituents between the stratosphere and troposphere. *J. Atmos. Sci.,* **37,** 994–1004.

——, 1981: Frontogenesis and geostrophically forced secondary circulations in the vicinity of jet stream-frontal zone systems. *J. Atmos. Sci.,* **38,** 954–973.

——, 1982: *Mesoscale Weather Systems of the Central United States.* CIRES/NOAA, University of Colorado, Boulder, CO 80309, 78 pp.

——, and P. J. Kennedy, 1981: Research aircraft measurements of jet stream geostrophic and ageostrophic winds. *J. Atmos. Sci.,* **38,** 2642–2652.

——, A. J. Krueger and P. J. Kennedy, 1982: Nowcasting the position and intensity of jet streams using a satellite-borne total ozone mapping spectrometer. *Nowcasting,* K. A. Browning, Ed., Academic Press, 137–145.

Staley, D. O., 1960: Evaluation of potential-vorticity changes near the tropopause and related vertical motions, vertical advection of vorticity, and transfer of radioactive debris from stratosphere to troposphere. *J. Meteor.,* **17,** 591–620.

Uccellini, L. W., R. A. Petersen, P. J. Kocin, M. J. Kaplan, J. W. Zack and V. C. Wong, 1983: Mesoscale numerical simulations of the Presidents' Day cyclone: Impact of sensible and latent heating on the pre-cyclogenetic environment. *Preprints 6th Conf. Numerical Weather Prediction,* Omaha, Amer. Meteor. Soc., 45–52.

——, P. J. Kocin, R. A. Petersen, C. H. Wash and K. F. Brill, 1984: The Presidents' Day cyclone of 18–19 February 1979: Synoptic overview and analysis of the subtropical jet streak influencing the pre-cyclogenetic period. *Mon. Wea. Rev.,* **112,** 31–55.

Whittaker, T. M., and R. A. Petersen, 1977: Objective cross-sectional analysis incorporating thermal enhancement of the observed winds. *Mon. Wea. Rev.,* **105,** 147–153.